

# Local Causality in a Friedmann-Robertson-Walker Spacetime

Joy Christian\*

*Einstein Centre for Local-Realistic Physics, 15 Thackley End, Oxford OX2 6LB, United Kingdom*

In the context of EPR-Bohm experiments and spin detections confined to spacelike hypersurfaces, a local, deterministic and realistic model within a Friedmann-Robertson-Walker spacetime with a constant spatial curvature ( $S^3$ ) is presented which describes simultaneous measurements of the spins of two fermions emerging in a singlet state from the decay of a spinless boson. Exact agreement with the probabilistic predictions of quantum theory is achieved in the model without data rejection, remote contextuality, superdeterminism or backward causation. A singularity-free Clifford-algebraic representation of  $S^3$  with vanishing spatial curvature and non-vanishing torsion is then employed to transform the model in a more elegant form. Several event-by-event numerical simulations of the model are presented, which confirm our analytical results with the accuracy of 4 parts in  $10^4$  parts.

## I. INTRODUCTION

Unlike our most fundamental theories of space and time, quantum theory happens to be incompatible with local causality. This fact was famously recognized in 1935 by Einstein, Podolsky, and Rosen (EPR) [1]. They hoped, however, that perhaps quantum mechanics can be completed into a locally causal theory by addition of supplementary (or “hidden”) parameters. Today such hopes of maintaining both locality and realism within physics seem to have been undermined by Bell’s theorem [2], with considerable support from experiments [3–9]. Bell set out to prove that no physical theory which is realistic as well as local in a sense espoused by Einstein can reproduce all of the statistical predictions of quantum mechanics. The purpose of this paper is to show that it is, in fact, possible to reproduce the statistical predictions of quantum states such as the EPR-Bohm state in a locally causal manner, in the familiar Friedmann-Robertson-Walker spacetime (albeit viewed as a *non*-cosmological solution of Einstein’s field equations). To demonstrate this, we shall follow the local-realistic framework proposed by Bell in his pioneering work [2] (which is reviewed in the Appendix below for convenience) using the powerful language of Geometric Algebra [10–12].

## II. TWO PARTICLES ENTANGLED IN THE SINGLET STATE

A locally causal description of the measurement of the spins of two spacelike separated spin- $\frac{1}{2}$  particles that are products of the decay of a single spin-zero particle has been considered by Bell [2]. Based on Bohm’s version of the EPR thought experiment, he considered a pair of spin- $\frac{1}{2}$  particles, moving freely after the decay in opposite directions, with particles 1 and 2 subject (respectively) to spin measurements along independently chosen unit directions  $\mathbf{a}$  and  $\mathbf{b}$ , which may be located at a spacelike distance from one another. If initially the emerging pair has vanishing total spin, then its quantum mechanical spin state can be described by the entangled singlet state,

$$|\Psi_{\mathbf{n}}\rangle = \frac{1}{\sqrt{2}} \left\{ |\mathbf{n}, +\rangle_1 \otimes |\mathbf{n}, -\rangle_2 - |\mathbf{n}, -\rangle_1 \otimes |\mathbf{n}, +\rangle_2 \right\}, \quad (1)$$

with  $\mathbf{n}$  as arbitrary direction and  $\boldsymbol{\sigma} \cdot \mathbf{n} |\mathbf{n}, \pm\rangle = \pm |\mathbf{n}, \pm\rangle$  describing the quantum mechanical eigenstates in which the particles have spin up or down in the units of  $\hbar = 2$ .

Our interest lies in an event-by-event reproduction of the probabilistic predictions of this entangled quantum state in a locally causal manner [2]. For any freely chosen measurement directions  $\mathbf{a}$  and  $\mathbf{b}$  in space there would be nine possible outcomes of the experiment in general, regardless of the distance between the directions. If we denote the angle between  $\mathbf{a}$  and  $\mathbf{b}$  by  $\eta_{\mathbf{ab}}$  and the local measurement results 0, +1, or –1 about these directions by  $\mathcal{A}$  and  $\mathcal{B}$ ,

---

\*Electronic address: jjc@alum.bu.edu

then quantum mechanics is well known to predict the following joint probabilities for these results:

$$P_{12}^{+-}(\eta_{\mathbf{ab}}) = P\{\mathcal{A} = +1, \mathcal{B} = -1 \mid \eta_{\mathbf{ab}}\} = \frac{1}{2} \cos^2\left(\frac{\eta_{\mathbf{ab}}}{2}\right), \quad (2)$$

$$P_{12}^{++}(\eta_{\mathbf{ab}}) = P\{\mathcal{A} = +1, \mathcal{B} = +1 \mid \eta_{\mathbf{ab}}\} = \frac{1}{2} \sin^2\left(\frac{\eta_{\mathbf{ab}}}{2}\right), \quad (3)$$

$$P_{12}^{-+}(\eta_{\mathbf{ab}}) = P_{12}^{+-}(\eta_{\mathbf{ab}}), \quad (4)$$

$$P_{12}^{--}(\eta_{\mathbf{ab}}) = P_{12}^{++}(\eta_{\mathbf{ab}}), \quad (5)$$

$$P_{12}^{+0}(\eta_{\mathbf{ab}}) = P_{12}^{-0}(\eta_{\mathbf{ab}}) = P_{12}^{0+}(\eta_{\mathbf{ab}}) = P_{12}^{0-}(\eta_{\mathbf{ab}}) = 0, \quad (6)$$

and

$$P_{12}^{00}(\eta_{\mathbf{ab}}) = 0, \quad (7)$$

where the superscript 0 indicates no detection and the subscripts 1 and 2 label the particles [13]. The probability that the spin of the particle 1 will be detected parallel to  $\mathbf{a}$  (regardless of whether particle 2 itself is detected) is also predicted by quantum mechanics. It is given by

$$P_1^+(\mathbf{a}) = P_1^-(\mathbf{a}) = \frac{1}{2}, \quad (8)$$

and likewise for particle 2 being detected parallel to  $\mathbf{b}$ . In what follows our goal is to demonstrate that, at least in the Friedmann-Robertson-Walker spacetime  $\mathbb{R} \times \Sigma$  with a constant spatial curvature, the above probabilities can be reproduced within the original local model of Bell [2].

### III. WITHIN THE SPATIAL SLICE OF FRIEDMANN-ROBERTSON-WALKER SPACETIME

To this end, consider a spacelike hypersurface  $\Sigma = S^3$  in a Friedmann-Robertson-Walker solution with  $\kappa = +1$ ,

$$ds^2 = dt^2 - a^2(t) d\Sigma^2, \quad d\Sigma^2 = \left[ \frac{d\rho^2}{1 - \kappa \rho^2} + \rho^2 d\Omega^2 \right], \quad (9)$$

where  $\Sigma = S^3$  can be recovered by introducing a new coordinate  $\chi = \sin^{-1}\rho$  (for a detailed derivation see section 22.8 of Ref. [14]). Here  $\rho$  is the radial coordinate. Now, for  $\kappa = +1$ , the tangent bundle of  $S^3$  happens to be trivial:  $TS^3 = S^3 \times \mathbb{R}^3$ . This renders the tangent space at each point of  $S^3$  to be isomorphic to  $\mathbb{R}^3$ . Thus local experiences of the experimenters within  $S^3$  are no different from those of their counterparts within  $\mathbb{R}^3$ . The global topology of  $S^3$ , however, is dramatically different from that of  $\mathbb{R}^3$ . In particular, the triviality of  $TS^3$  means that  $S^3$  is parallelizable [15]. Therefore, a global *anholonomic* frame can be specified on  $S^3$  that fixes each of its points uniquely [15, 16]. Such a frame renders  $S^3$  diffeomorphic to the group  $SU(2)$  — *i.e.*, to the set of all unit quaternions:

$$S^3 = \left\{ \mathbf{H}(I \cdot \mathbf{v}, \eta) \mid \|\mathbf{H}(I \cdot \mathbf{v}, \eta)\| = 1 \right\}. \quad (10)$$

Here we have parameterized each quaternion  $\mathbf{H} \in S^3$  as

$$\mathbf{H}(I \cdot \mathbf{v}, \eta) = \exp\{(I \cdot \mathbf{v})\eta\} \quad (11)$$

such that  $I \cdot \mathbf{v}$ , with a trivector  $I$ , is a bivector rotating about some vector  $\mathbf{v} \in \mathbb{R}^3$ , and  $\eta$  is half of the angle by which  $\mathbf{H}$  stands rotated about  $\mathbf{v}$ . As in these definitions, in what follows we will be using the notation of geometric algebra [10, 16, 17]. Accordingly, all vector fields in  $\mathbb{R}^3$  such as  $\mathbf{v}$  and  $\mathbf{w}$  will be assumed to satisfy the geometric product

$$\mathbf{v} \mathbf{w} = \mathbf{v} \cdot \mathbf{w} + \mathbf{v} \wedge \mathbf{w}, \quad (12)$$

with the duality relation  $\mathbf{v} \wedge \mathbf{w} = I \cdot (\mathbf{v} \times \mathbf{w})$ . In the next steps it will be useful to recall that  $(\mathbf{v} \wedge \mathbf{w})^\dagger = -(\mathbf{v} \wedge \mathbf{w})$ .

Since we are primarily concerned with a galactic, solar, or terrestrial scenario, in what follows we will restrict our attention to the current epoch of the cosmos by setting the scale factor  $a(t) = 1$  in the solution (9). Moreover, we will

not be using the time coordinate in (9) explicitly. Instead, we will follow the practice of defining the measurement events in terms of the initial and final instants of time as usually done within the context of Bell's local model [2, 3]. Readers who are not familiar with the above practice are urged to review the Appendix below before proceeding further. We also postpone the full spacetime covariant investigation of local causality until section VI, where we show how and why only the spacelike components of the relativistic spins enter the calculations of EPR correlations even though the two spins themselves emerge relativistically from the overlap of the backward light cones of Alice and Bob.

Consider now two unit quaternions from the closed set  $S^3$ , say  $\mathbf{P}_o(\mathbf{n} \wedge \mathbf{e}_o, \eta_{\mathbf{n}\mathbf{e}_o})$  and  $\mathbf{Q}_o(\mathbf{z} \wedge \mathbf{s}_o, \eta_{\mathbf{z}\mathbf{s}_o})$ , defined as

$$\mathbf{P}_o = \cos(\eta_{\mathbf{n}\mathbf{e}_o}) + \frac{\mathbf{n} \wedge \mathbf{e}_o}{\|\mathbf{n} \wedge \mathbf{e}_o\|} \sin(\eta_{\mathbf{n}\mathbf{e}_o}) \quad (13)$$

and

$$\mathbf{Q}_o = \cos(\eta_{\mathbf{z}\mathbf{s}_o}) + \frac{\mathbf{z} \wedge \mathbf{s}_o}{\|\mathbf{z} \wedge \mathbf{s}_o\|} \sin(\eta_{\mathbf{z}\mathbf{s}_o}), \quad (14)$$

where  $\mathbf{n} \in T_p S^3 \cong \mathbb{R}^3$  is an arbitrary unit vector in the tangent space  $T_p S^3$  at some point  $p$  of  $S^3$ ,  $\mathbf{z}$  is a fixed reference vector in  $T_q S^3$  at a different point  $q$  of  $S^3$ , and  $\mathbf{e}_o$  and  $\mathbf{s}_o$  are two other tangential vectors in  $T_q S^3$ . Here the bivector  $I \cdot \mathbf{e}_o$  may be thought of as representing an individual spin within the pair of decaying particles in the singlet state, and the bivector  $I \cdot \mathbf{s}_o$  may be thought of as representing the spin of the composite pair [13]. Note that, although  $\mathbf{P}_o$  and  $\mathbf{Q}_o$  are normalized to unity, their sum  $\mathbf{P}_o + \mathbf{Q}_o$  need not be. In fact, they satisfy the following triangle inequality for arbitrary pairs of such quaternions,

$$\|\mathbf{P}_o + \mathbf{Q}_o\| \leq \|\mathbf{P}_o\| + \|\mathbf{Q}_o\|, \quad (15)$$

reflecting the metrical structure of  $S^3$ . Moreover, since  $S^3$  is closed under multiplication, we also have  $\|\mathbf{P}_o \mathbf{Q}_o\| = 1$ .

Within the freedom provided by this inequality, the above constraints lead us to the following choice for the set of initial (or *complete* [2]) states  $(\mathbf{P}_o, \mathbf{Q}_o)$  of our physical system:

$$\Lambda = \left\{ (\mathbf{P}_o, \mathbf{Q}_o) \mid \|\mathbf{P}_o + \mathbf{Q}_o\| = \mathcal{N}(\eta_{\mathbf{n}\mathbf{e}_o}, \eta_{\mathbf{z}\mathbf{s}_o}) \quad \forall \mathbf{n} \right\}, \quad (16)$$

with the value  $\mathcal{N}$  of the norm given by the *ansatz*

$$\mathcal{N}(\eta_{\mathbf{n}\mathbf{e}_o}, \eta_{\mathbf{z}\mathbf{s}_o}) = 1 + \sin^2(\eta_{\mathbf{n}\mathbf{e}_o}) + \left[ -1 + \frac{2}{\sqrt{1 + 3 \left( \frac{\eta_{\mathbf{z}\mathbf{s}_o}}{\kappa\pi} \right)}} \right]^2, \quad (17)$$

which is necessarily a function of the variable angles  $\eta_{\mathbf{n}\mathbf{e}_o}$  and  $\eta_{\mathbf{z}\mathbf{s}_o}$ . It represents a local-realistic counterpart of the singlet state (1). It would be different, for example, for a mixed state<sup>1</sup>, or for any quantum state other than (1). Note also that we have allowed all three possible curvatures of  $\Sigma$ , with  $\kappa = -1$  being equivalent to  $\eta_{\mathbf{z}\mathbf{s}_o} \rightarrow 2\pi - \eta_{\mathbf{z}\mathbf{s}_o}$ . The significance of this form of  $\mathcal{N}$  will become clear soon.

If we now substitute expression (17) into the inequality

$$\|\mathbf{P}_o\|^2 \geq \|\mathbf{P}_o + \mathbf{Q}_o\| - 1, \quad (18)$$

which follows from multiplying the inequality (15) with  $\|\mathbf{P}_o\| = 1$  on both sides and simplifying, then [upon using

$$\|\mathbf{P}_o\|^2 = \cos^2(\eta_{\mathbf{n}\mathbf{e}_o}) + \sin^2(\eta_{\mathbf{n}\mathbf{e}_o}) \quad (19)$$

---

<sup>1</sup> The analysis presented in this paper is generalizable to mixed states. However, the *ansatz* for the norm  $\mathcal{N}$  appearing in Eq. (17) would be different for a mixed state [or any quantum state other than (1)], depending on the detailed characteristics of the mixed state. It is beyond the scope and purpose of this paper to investigate the question of mixed states further. The goal of the paper is to investigate local causality for the pure singlet state (1) within the context of Bell's theorem, because that is the quantum state considered in the proof of Bell's theorem [2]. It is not the goal of the present paper to reproduce all quantum mechanical predictions for any quantum state. Moreover, unlike the pure entangled state (1), any mixture of product states will not yield correlations as strong as (1) does (i.e., correlations will not deviate much from linear correlations). Therefore mixed states are of little interest in the context of Bell's theorem.

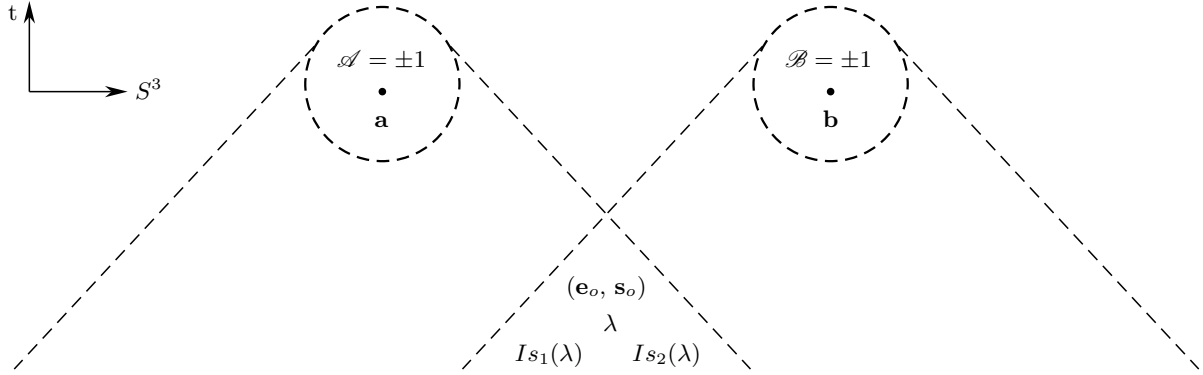


FIG. 1: The local results  $\mathcal{A}(\mathbf{a}; \mathbf{e}_o, \mathbf{s}_o)$  and  $\mathcal{B}(\mathbf{b}; \mathbf{e}_o, \mathbf{s}_o)$  are deterministically brought about by the initial state  $(\mathbf{e}_o, \mathbf{s}_o)$ . In the Clifford-algebraic representation of the local model considered below, the initial state is a possible orientation  $\lambda$  of the 3-sphere.

from Eq. (13)] the triangle inequality (15) simplifies to

$$|\cos(\eta_{\mathbf{n}\mathbf{e}_o})| \geq -1 + \frac{2}{\sqrt{1 + 3\left(\frac{\eta_{\mathbf{z}\mathbf{s}_o}}{\kappa\pi}\right)}}. \quad (20)$$

In what follows it is very important to recognize that this constraint is simply an expression of the intrinsic metrical and topological structures of  $S^3$ , and as such it holds for *all* vectors  $\mathbf{n}$  for a given pair of initial states  $(\mathbf{e}_o, \mathbf{s}_o)$ ; and, conversely, for *all* pairs of initial states  $(\mathbf{e}_o, \mathbf{s}_o)$  for a given choice of vector  $\mathbf{n}$ . This can be easily verified by starting, for example, with a different pair of quaternions, say with the pair  $\mathbf{P}'_o(\mathbf{n}' \wedge \mathbf{e}_o, \eta_{\mathbf{n}'\mathbf{e}_o})$  and  $\mathbf{Q}_o(\mathbf{z} \wedge \mathbf{s}_o, \eta_{\mathbf{z}\mathbf{s}_o})$ , where

$$\mathbf{P}'_o = \cos(\eta_{\mathbf{n}'\mathbf{e}_o}) + \frac{\mathbf{n}' \wedge \mathbf{e}_o}{\|\mathbf{n}' \wedge \mathbf{e}_o\|} \sin(\eta_{\mathbf{n}'\mathbf{e}_o}), \quad (21)$$

and arriving at a similar constraint as the one in Eq. (20):

$$|\cos(\eta_{\mathbf{n}'\mathbf{e}_o})| \geq -1 + \frac{2}{\sqrt{1 + 3\left(\frac{\eta_{\mathbf{z}\mathbf{s}_o}}{\kappa\pi}\right)}}. \quad (22)$$

This procedure can then be repeated for *all* vectors  $\mathbf{n}'$ , and—for a given vector  $\mathbf{n}$ —for *all* pairs of states  $(\mathbf{e}'_o, \mathbf{s}'_o)$ .

If we now let  $\mathbf{e}_o \in T_q S^3$  and  $\mathbf{s}_o \in T_q S^3$  be two random vectors, uniformly distributed over  $S^2$ , and let  $\eta_{\mathbf{z}\mathbf{s}_o}$  be a random scalar, uniformly distributed over  $[0, \pi]$ , then we can simplify the set (16) of complete or initial states as

$$\Lambda = \left\{ (\mathbf{P}_o, \mathbf{Q}_o) \left| |\cos(\eta_{\mathbf{n}\mathbf{e}_o})| \geq -1 + \frac{2}{\sqrt{1 + 3\left(\frac{\eta_{\mathbf{z}\mathbf{s}_o}}{\kappa\pi}\right)}} \forall \mathbf{n} \right. \right\}. \quad (23)$$

By the previous results this set is invariant under the rotations of  $\mathbf{n}$ . Consequently, we identify  $\mathbf{n}$  as a detector direction, and define the measurement events observed by (say) Alice and Bob—along their *freely chosen* detector directions  $\mathbf{n} = \mathbf{a}$  and  $\mathbf{n} = \mathbf{b}$ —by two functions of the form

$$\pm 1 = \mathcal{A}(\mathbf{a}; \mathbf{e}_o, \mathbf{s}_o): \mathbb{R}^3 \times \Lambda \longrightarrow S^3 \cong \text{SU}(2) \quad (24)$$

and

$$\pm 1 = \mathcal{B}(\mathbf{b}; \mathbf{e}_o, \mathbf{s}_o): \mathbb{R}^3 \times \Lambda \longrightarrow S^3 \cong \text{SU}(2). \quad (25)$$

These functions are identical to those considered by Bell [2] apart from the choice of their codomain, which is now the compact space  $S^3$  instead of a subset of  $\mathbb{R}$ . That such maps indeed exist can be seen easily by noting that  $\mathbf{P}_o \rightarrow \pm 1$  as  $\eta_{\mathbf{n}\mathbf{e}_o} \rightarrow 0$  or  $\pi$ . More explicitly, we construct

$$S^3 \ni \pm 1 = \mathcal{A}(\mathbf{a}; \mathbf{e}_o, \mathbf{s}_o) = -\text{sign}\{\cos(\eta_{\mathbf{a}\mathbf{e}_o})\} \text{ for a given } \mathbf{s}_o \quad (26)$$

and

$$S^3 \ni \pm 1 = \mathcal{B}(\mathbf{b}; \mathbf{e}_o, \mathbf{s}_o) = + \text{sign}\{\cos(\eta_{\mathbf{b}\mathbf{e}_o})\} \text{ for the same } \mathbf{s}_o. \quad (27)$$

Evidently, these functions define strictly local, realistic, and deterministically determined measurement events. Apart from the common cause  $(\mathbf{e}_o, \mathbf{s}_o)$ , which originates in the overlap of the backward lightcones of Alice and Bob as shown in Fig. 1, the event  $\mathcal{A} = \pm 1$  depends *only* on the measurement direction  $\mathbf{a}$  chosen freely by Alice; and analogously, apart from the common cause  $(\mathbf{e}_o, \mathbf{s}_o)$ , the event  $\mathcal{B} = \pm 1$  depends *only* on the measurement direction  $\mathbf{b}$  chosen freely by Bob. In particular, the function  $\mathcal{A}(\mathbf{a}; \mathbf{e}_o, \mathbf{s}_o)$  *does not* depend on either  $\mathbf{b}$  or  $\mathcal{B}$ , and the function  $\mathcal{B}(\mathbf{b}; \mathbf{e}_o, \mathbf{s}_o)$  *does not* depend on either  $\mathbf{a}$  or  $\mathcal{A}$ , just as demanded by Bell's formulation of local causality [2].

#### IV. CALCULATION OF JOINT PROBABILITY FOR OBSERVING MEASUREMENT EVENTS

Now, to calculate the joint probabilities for observing the events  $\mathcal{A} = \pm 1$  and  $\mathcal{B} = \pm 1$  simultaneously along the directions  $\mathbf{a}$  and  $\mathbf{b}$ , we follow the well known analysis carried out by Pearle for a formally similar local model [13]. Pearle begins by representing each pair of decaying particles by a point  $\mathbf{r}$  in a state space made out of a ball of unit radius in  $\mathbb{R}^3$ . His state space is thus a well known representation of the group  $\text{SO}(3)$ , each point of which corresponding to a rotation, with the direction  $\mathbf{r}$  of length  $0 \leq r \leq 1$  from the origin representing the axis of rotation and the angle  $\pi r$  representing the angle of rotation. The identity rotation corresponds to the point at the center of the ball. If we now identify the boundaries of two such unit balls, then we recover our 3-sphere, diffeomorphic to the double covering group of  $\text{SO}(3)$ , namely  $\text{SU}(2)$ . The pair of particles in this state space is represented by the quaternion  $\mathbf{Q}_o$  defined in Eq. (14), which is rotating about the axis  $\frac{\mathbf{z} \times \mathbf{s}_o}{\|\mathbf{z} \times \mathbf{s}_o\|}$  by the angle  $2\eta_{\mathbf{z}\mathbf{s}_o}$ , with the unit vector  $\mathbf{s}_o$  sweeping a 2-sphere within the 3-sphere [16, 17].

The relationship between the rotation angle  $\pi r$  within Pearle's state space  $\text{SO}(3)$  and the rotation angle  $2\eta_{\mathbf{z}\mathbf{s}_o}$  within our state space  $\text{SU}(2) \cong S^3$  turns out to be simple:

$$\cos\left(\frac{\pi}{2}r\right) = \begin{cases} -1 + \frac{2}{\sqrt{1 + 3\left(\frac{\eta_{\mathbf{z}\mathbf{s}_o}}{\kappa\pi}\right)}} = f(\eta_{\mathbf{z}\mathbf{s}_o}), \\ -1 + \frac{2}{\sqrt{4 - 3\left(\frac{\eta_{\mathbf{z}\mathbf{s}_o}}{\kappa\pi}\right)}} = f(\pi - \eta_{\mathbf{z}\mathbf{s}_o}). \end{cases} \quad (28)$$

This can be recognized by first solving Eq. (28) for  $\frac{\eta_{\mathbf{z}\mathbf{s}_o}}{\kappa\pi}$  and then differentiating the solution with respect to  $r$ , which gives the probability density worked out by Pearle:

$$p(r) = \frac{1}{\kappa\pi} \frac{d\eta_{\mathbf{z}\mathbf{s}_o}(r)}{dr} = \frac{4\pi}{3} \frac{\sin\left(\frac{\pi}{2}r\right)}{\left\{1 + \cos\left(\frac{\pi}{2}r\right)\right\}^3}, \quad 0 \leq r \leq 1. \quad (30)$$

This function specifies the distribution of probability that a pair of particles is represented by the point  $\mathbf{r}$  in the unit ball. Integrating this distribution from 0 to  $r$  we may also obtain the cumulative probability distribution in the ball:

$$C(r) = \int_0^r p(u) du = -\frac{1}{3} + \frac{4}{3 \left\{1 + \cos\left(\frac{\pi}{2}r\right)\right\}^2}. \quad (31)$$

This function specifies the probability of finding the pair in any state up to the state  $\mathbf{r}$  within Pearle's state space. From solving Eq. (28) we see, however, that it is equal to our ratio  $\frac{\eta_{\mathbf{z}\mathbf{s}_o}}{\kappa\pi}$ , and therefore also specifies the probability of finding the pair in any initial state up to the state  $\mathbf{s}_o$ .

For a given reference vector  $\mathbf{z}$ , the above relations allow us to translate between our representation in terms of the states  $(\mathbf{e}_o, \mathbf{s}_o)$  in  $\text{SU}(2)$  and Pearle's representation in terms of the states  $\mathbf{r}$  in  $\text{SO}(3)$ . We can therefore rewrite our geometrical constraint (20) in terms of his state  $\mathbf{r}$  as

$$|\cos(\eta_{\mathbf{a}\mathbf{e}_o})| \geq \cos\left(\frac{\pi}{2}r\right) \quad \text{and} \quad |\cos(\eta_{\mathbf{b}\mathbf{e}_o})| \geq \cos\left(\frac{\pi}{2}r\right), \quad (32)$$

where our vector  $\mathbf{e}_o$  is related to his vector  $\mathbf{r}$  as  $\mathbf{e}_o = \mathbf{r}/r$ . We are thus treating the axis  $\mathbf{e}_o$  and the angle  $\pi r$  of the rotation of the spin as two independent random variables.

The equalities in the above inequalities correspond to the boundaries of the two circular caps on the spherical surface of radius  $r$  within the SO(3) ball considered by Pearle. The intersection of the two circular caps is then

$$\mathcal{I}(\pi r, \eta_{\mathbf{ab}}) = 4r^2 \int_{\frac{\eta_{\mathbf{ab}}}{2}}^{\frac{\pi}{2}r} d\xi \sqrt{1 - \left\{ \frac{\cos\left(\frac{\pi}{2}r\right)}{\cos(\xi)} \right\}^2} \quad \text{if } \eta_{\mathbf{ab}} \leq \pi r, \quad (33)$$

and zero otherwise. This area is derived by Pearle in the Appendix A of his paper. It is, however, not the correct overlap area for our model. What has been overlooked in Pearle's derivation are the contributions to  $\mathcal{I}(\pi r, \eta_{\mathbf{ab}})$  from the *relative* rotations of the state  $\mathbf{e}_o = \mathbf{r}/r$  along the directions  $\mathbf{a}$  and  $\mathbf{b}$ . While the state  $\mathbf{e}_o$  can be common to both  $\mathbf{a}$  and  $\mathbf{b}$ , the corresponding rotations  $\pi r$  cannot be the same in general about both  $\mathbf{a}$  and  $\mathbf{b}$ . An example of the difference can be readily seen from the relations (28) and (29), while heeding to the double covering in SU(2):

$$\pi \Delta r = \begin{cases} 2 \cos^{-1} \left[ -1 + \frac{2}{\sqrt{1 + 3 \left( \frac{\eta_{\mathbf{ab}}}{\pi} \right)}} \right] & \text{if } 0 \leq \eta_{\mathbf{ab}} \leq \frac{\pi}{2}, \\ 2 \cos^{-1} \left[ -1 + \frac{2}{\sqrt{4 - 3 \left( \frac{\eta_{\mathbf{ab}}}{\pi} \right)}} \right] & \text{if } \frac{\pi}{2} \leq \eta_{\mathbf{ab}} \leq \pi. \end{cases} \quad (34)$$

Evidently,  $\Delta r = 0$  when  $\eta_{\mathbf{ab}} = 0$  or  $\pi$ , and maximum when  $\eta_{\mathbf{ab}} = \frac{\pi}{2}$ . More generally, the effective radius of the spherical surface to which the circular caps belong must be "phase-shifted" to  $r' = r \sqrt{h(\eta_{\mathbf{ab}})}$  in our SU(2) model, where

$$h(\eta_{\mathbf{ab}}) = \frac{3\pi}{8} \left\{ \frac{\sin^2(\eta_{\mathbf{ab}})}{\pi \sin^2\left(\frac{1}{2}\eta_{\mathbf{ab}}\right) + \eta_{\mathbf{ab}} \cos(\eta_{\mathbf{ab}}) - \sin(\eta_{\mathbf{ab}})} \right\} \quad (35)$$

is the inverse of the function derived in Pearle's Eq. (23). The correct overlap area is then obtained by replacing  $r$  by  $r'$  in the differential area  $dA = r^2 d\omega$  in Eq. (33) so that

$$\mathcal{I}(\pi r, \eta_{\mathbf{ab}}) \longrightarrow \mathcal{J}(\pi r, \eta_{\mathbf{ab}}) = h(\eta_{\mathbf{ab}}) \mathcal{I}(\pi r, \eta_{\mathbf{ab}}). \quad (36)$$

Using the probability density (30) and the overlap area (36), we can now calculate various joint probabilities as

$$\begin{aligned} P_{12}^{+-}(\eta_{\mathbf{ab}}) &= P_{12}^{-+}(\eta_{\mathbf{ab}}) = \int_{\frac{\eta_{\mathbf{ab}}}{\pi}}^1 p(r) \frac{\mathcal{J}(\pi r, \eta_{\mathbf{ab}})}{4\pi r^2} dr \\ &= \frac{1}{2} \cos^2\left(\frac{\eta_{\mathbf{ab}}}{2}\right) \end{aligned} \quad (37)$$

and

$$\begin{aligned} P_{12}^{++}(\eta_{\mathbf{ab}}) &= P_{12}^{--}(\eta_{\mathbf{ab}}) = \int_{1-\frac{\eta_{\mathbf{ab}}}{\pi}}^1 p(r) \frac{\mathcal{J}(\pi r, \pi - \eta_{\mathbf{ab}})}{4\pi r^2} dr \\ &= \frac{1}{2} \sin^2\left(\frac{\eta_{\mathbf{ab}}}{2}\right). \end{aligned} \quad (38)$$

These calculations of the joint probabilities are analogous to those by Pearle, except for using the area  $\mathcal{J}(\pi r, \eta_{\mathbf{ab}})$ . In particular, since  $h(\eta_{\mathbf{ab}})$  expressed in (35) is an inverse of the function derived in Pearle's Eq. (23), our equations (37) and (38) follow at once from Pearle's equations (5) and (6), respectively, upon multiplying through with  $h(\eta_{\mathbf{ab}})$ .

Although the statistical effects of the constraints (32) in our model turn out to be almost identical to those in Pearle's model, the characteristics of the two models are markedly different. In our model the vectors  $\mathbf{e}_o$  and  $\mathbf{s}_o$  ensure in tandem that there are no initial states for which

$$|\cos(\eta_{\mathbf{ne}_o})| < \cos\left(\frac{\pi}{2}r\right) = -1 + \frac{2}{\sqrt{1 + 3 \left( \frac{\eta_{\mathbf{zs}_o}}{\kappa\pi} \right)}}. \quad (39)$$

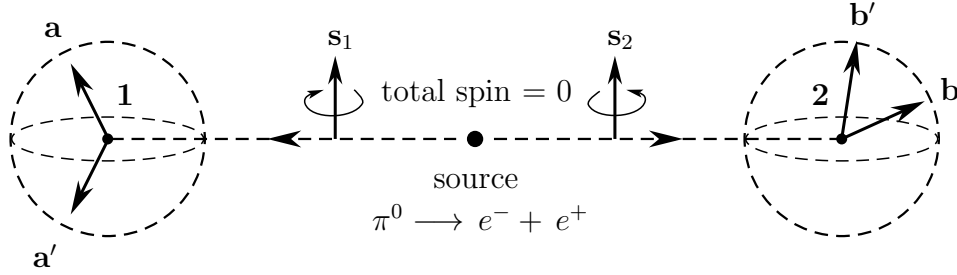


FIG. 2: A spin-less neutral pion decays into an electron-positron pair (such a photon-less decay is quite rare but not impossible, and will suffice for our theoretical purposes here [12]). Measurements of spin components on each separated fermion are performed at remote stations **1** and **2**, providing binary outcomes along arbitrary directions such as **a** and **b** [cf. Eq. (69)].

Consequently, the detectors of Alice and Bob can receive the spin states  $\mathbf{e}_o$  only if the constraints (32) are satisfied. In other words, unlike Pearle’s model, our model is not concerned about data rejection or detection loophole. In particular, in our model the fraction  $g(\eta_{\mathbf{ab}})$  of events in which both particles are detected is exactly equal to 1:

$$g(\eta_{\mathbf{ab}}) = \frac{P_{12}^{+-}(\eta_{\mathbf{ab}})}{\frac{1}{2} \cos^2\left(\frac{\eta_{\mathbf{ab}}}{2}\right)} = \frac{P_{12}^{++}(\eta_{\mathbf{ab}})}{\frac{1}{2} \sin^2\left(\frac{\eta_{\mathbf{ab}}}{2}\right)} = 1 \quad \forall \eta_{\mathbf{ab}} \in [0, \pi]. \quad (40)$$

Clearly, a measurement event cannot occur if there does not exist a state which can bring about that event. Since the initial state of the system is specified by the pair  $(\mathbf{e}_o, \mathbf{s}_o)$  and not just by the vector  $\mathbf{e}_o$ , there are no states of the system for which  $|\cos(\eta_{\mathbf{n}\mathbf{e}_o})| < f(\eta_{\mathbf{z}\mathbf{s}_o})$  for *any* vector  $\mathbf{n}$ . Thus a measurement event cannot occur for  $|\cos(\eta_{\mathbf{n}\mathbf{e}_o})| < f(\eta_{\mathbf{z}\mathbf{s}_o})$ , no matter what  $\mathbf{n}$  is. As a result, there is a one-to-one correspondence between the initial state  $(\mathbf{e}_o, \mathbf{s}_o)$  selected from the set (23) and the measurement events  $\mathcal{A}$  and  $\mathcal{B}$  specified by the Eqs. (26) and (27). This means, in particular, that the “fraction”  $g(\eta_{\mathbf{ab}})$  in our model is equal to 1 for all  $\eta_{\mathbf{ab}}$ , dictating the vanishing of the probabilities

$$P_{12}^{00}(\eta_{\mathbf{ab}}) = 1 + g(\eta_{\mathbf{ab}}) - 2g(0) = 0, \quad (41)$$

which follows from Pearle’s Eq. (9). Moreover, from his Eq. (8) we also have  $P_{12}^{+0}(\eta_{\mathbf{ab}}) = \frac{1}{2}[g(0) - g(\eta_{\mathbf{ab}})]$ , giving

$$P_{12}^{+0}(\eta_{\mathbf{ab}}) = P_{12}^{-0}(\eta_{\mathbf{ab}}) = P_{12}^{+0}(\eta_{\mathbf{ab}}) = P_{12}^{-0}(\eta_{\mathbf{ab}}) = 0. \quad (42)$$

Together with the probabilities for individual detections,

$$P_1^+(\mathbf{a}) = P_1^-(\mathbf{a}) = P_2^+(\mathbf{b}) = P_2^-(\mathbf{b}) = \frac{1}{2}g(0) = \frac{1}{2}, \quad (43)$$

the correlation between  $\mathcal{A}$  and  $\mathcal{B}$  then works out to be

$$\begin{aligned} \mathcal{E}(\mathbf{a}, \mathbf{b}) &= \lim_{n \gg 1} \left[ \frac{1}{n} \sum_{i=1}^n \mathcal{A}(\mathbf{a}; \mathbf{e}_o^i, \mathbf{s}_o^i) \mathcal{B}(\mathbf{b}; \mathbf{e}_o^i, \mathbf{s}_o^i) \right] \\ &= \frac{P_{12}^{++} + P_{12}^{--} - P_{12}^{+-} - P_{12}^{-+}}{P_{12}^{++} + P_{12}^{--} + P_{12}^{+-} + P_{12}^{-+}} \\ &= -\cos(\eta_{\mathbf{ab}}). \end{aligned} \quad (44)$$

Since all of the probabilities predicted by our local model in  $S^3$  match exactly with the corresponding predictions of quantum mechanics, the violations of not only the CHSH inequality, but also Clauser-Horne inequality follow [3, 17].

## V. EVENT-BY-EVENT NUMERICAL SIMULATIONS OF THE STRONG CORRELATIONS

We have verified the above results in several event-by-event numerical simulations [19, 20], which provide further insights into the strength of the correlation for different values of  $\kappa$ . As we discussed above, the rotation angle  $\eta_{\mathbf{z}\mathbf{s}_o}$

and the cumulative distribution function  $C(r)$  are related by  $\kappa$  as

$$\frac{\eta_{\mathbf{z}\mathbf{s}_o}}{\pi} = \kappa C(r), \quad (45)$$

where  $|\kappa| \leq \infty$  can be interpreted as a *strength constant*. It is easy to verify in the simulations [19, 20] that EPR-Bohm correlation results for  $\kappa = +1$ , whereas linear correlation results for  $\kappa = 0$ . The unphysical, or PR box correlation can also be generated in the simulation by letting  $\kappa > +1$ . On the other hand, setting  $\kappa = -1$  [which is equivalent to letting  $\eta_{\mathbf{z}\mathbf{s}_o} \rightarrow 2\pi - \eta_{\mathbf{z}\mathbf{s}_o}$  in Eq. (20)] leads back to the linear correlation [19, 20]. The crucial observation here is that the strong, or quantum correlations are manifested only for  $\kappa = +1$ . Consequently, they can be best understood as resulting from the geometrical and topological structures of the quaternionic  $S^3$ , as defined, for example, in Eq. (10).

This conclusion can be further substantiated by first reflecting on a non-quaternionic or vector representation of the 3-sphere to model rotations, and then returning back to the quaternionic representation to appreciate the difference. It is well known that tensors such as ordinary vectors are not capable of modelling rotations in the physical space, let alone modelling spinors in a singularity-free manner [16, 17]. However, in the present context we are not interested in modelling all possible rotations and their all possible compositions in the physical space. We are only interested in establishing the correct correlation between some very special limiting points of the 3-sphere, namely between its scalar points such as  $\mathcal{A}(\mathbf{a}, \lambda) = \pm 1$  and  $\mathcal{B}(\mathbf{b}, \lambda) = \pm 1$ , with  $\lambda$  being the “hidden variable” in the sense of Bell [2, 16, 17]. It turns out that in that case we can indeed model rotations (or more precisely, their spin values) by means of ordinary vectors and their inner products, but not with a single Riemannian metric [20]. A one-parameter family of *effective* metrics is required to model the relative spin values correctly. Given two vectors  $\mathbf{u}$  and  $\mathbf{v}$ , their inner product  $g(\mathbf{u}, \mathbf{v}, \eta)$  is defined by the constraint  $|\cos(\mathbf{u}, \mathbf{v})| \geq f(\eta) \in [0, 1]$ , with the two extreme cases, namely  $|\cos(\mathbf{u}, \mathbf{v})| \geq 0$  and  $|\cos(\mathbf{u}, \mathbf{v})| \geq 1$ , quantifying the weakest and the strongest topologies, respectively. Here the weakest topology dictated by  $|\cos(\mathbf{u}, \mathbf{v})| \geq 0$  is the topology of  $\mathbb{R}^3$ , where relatively few vectors  $\mathbf{u}$  and  $\mathbf{v}$  are orthogonal to each other. The strongest topology dictated by  $|\cos(\mathbf{u}, \mathbf{v})| \geq 1$ , on the other hand, is more interesting, since in that case nearly *all* of the vectors  $\mathbf{u}$  and  $\mathbf{v}$  are orthogonal to each other. All intermediate topologies are dictated by *the effective metric*

$$g(\mathbf{u}, \mathbf{v}, \eta) = \begin{cases} \mathbf{u} \cdot \mathbf{v} & \text{if } |\mathbf{u} \cdot \mathbf{v}| \geq f(\eta) \\ 0 & \text{if } |\mathbf{u} \cdot \mathbf{v}| < f(\eta), \end{cases} \quad (46)$$

where

$$f(\eta) := -1 + \frac{2}{\sqrt{1 + 3\left(\frac{\eta}{\pi}\right)}} \quad \text{with } \eta \in [0, \pi], \quad \text{and } \mathbf{u} \cdot \mathbf{v} := \cos(\mathbf{u}, \mathbf{v}). \quad (47)$$

Evidently, the orthogonality of the vectors  $\mathbf{u}$  and  $\mathbf{v}$  is defined here by the condition  $g(\mathbf{u}, \mathbf{v}, \eta) = 0$ , depending on the parameter  $\eta \in [0, \pi]$ . It is this one-parameter family of metrics that has been implemented in the simulations [19, 20]. The slight change in notation of the distribution function from that in Eq. (20) is purely for the coding convenience.

## VI. DERIVATION OF THE STRONG CORRELATIONS USING GEOMETRIC ALGEBRA

Returning to the singularity-free representation of  $S^3$  specified in Eqs. (10) to (14), it is worth recalling that angular momenta are best described, not by ordinary polar vectors, but by pseudo-vectors, or bivectors, that change sign upon reflection [16]. One only has to compare a spinning object, like a barber’s pole, with its image in a mirror to appreciate this elementary fact. The mirror image of a polar vector representing the spinning object is not the polar vector that represents the mirror image of the spinning object. In fact it is the negative of the polar vector that does the job. Therefore the spin angular momenta considered previously are better represented by a set of unit bivectors using the powerful language of geometric algebra [10]. They can be expressed in terms of graded bivector bases with sub-algebra

$$L_i(\lambda) L_j(\lambda) = -\delta_{ij} - \sum_k \epsilon_{ijk} L_k(\lambda), \quad (48)$$

which span a tangent space at each point of  $S^3$ , with a choice of orientation  $\lambda = \pm 1$ . Contracting this equation on both sides with the components  $a^i$  and  $b^j$  of arbitrary unit vectors  $\mathbf{a}$  and  $\mathbf{b}$  then gives the convenient bivector identity

$$\mathbf{L}(\mathbf{a}, \lambda) \mathbf{L}(\mathbf{b}, \lambda) = -\mathbf{a} \cdot \mathbf{b} - \mathbf{L}(\mathbf{a} \times \mathbf{b}, \lambda), \quad (49)$$



which is simply a geometric product between the unit bivectors representing the spin momenta considered previously:

$$\mathbf{L}(\mathbf{a}, \lambda) = \lambda I \mathbf{a} = \lambda I \cdot \mathbf{a} \equiv \lambda(\mathbf{e}_x \wedge \mathbf{e}_y \wedge \mathbf{e}_z) \cdot \mathbf{a} = (\pm 1 \text{ spin about the direction } \mathbf{a}) \quad (50)$$

and<sup>2</sup>

$$\mathbf{L}(\mathbf{b}, \lambda) = \lambda I \mathbf{b} = \lambda I \cdot \mathbf{b} \equiv \lambda(\mathbf{e}_x \wedge \mathbf{e}_y \wedge \mathbf{e}_z) \cdot \mathbf{b} = (\pm 1 \text{ spin about the direction } \mathbf{b}), \quad (51)$$

where the trivector  $I := \mathbf{e}_x \wedge \mathbf{e}_y \wedge \mathbf{e}_z$  with  $I^2 = -1$  represents the volume form on  $S^3$  and ensures that  $\mathbf{L}^2(\mathbf{n}, \lambda) = -1$ .

In the above representation of spins we have used algebra  $Cl_{3,0}$  of the three-dimensional physical space [10]. However, as shown in Fig. 1, in the EPR-Bohm type experiments the initial state  $\lambda$  of the singlet system originates in the overlap of the backward light cones of Alice and Bob. The constituent spins emerging from the source are then detected at a spacelike distance from each other at a later time, as shown in Fig. 2. Therefore, full relativistic considerations are essential in the analysis of local causality in the present context, as Bell has explained in Ref. [21]. For that purpose, the appropriate algebra is  $Cl_{1,3}$ . It is also known as ‘‘spacetime algebra’’, or STA [22]. Within spacetime algebra  $Cl_{1,3}$ , we now represent the two constituent spins by using 4-vectors, as  $Is_1(\lambda) = Is_1^\mu(\lambda)\gamma_\mu$  and  $Is_2(\lambda) = Is_2^\mu(\lambda)\gamma_\mu$ , where the set  $\{\gamma_0, \gamma_1, \gamma_2, \gamma_3\}$  of  $\gamma$ -vectors forms an orthonormal basis, and its elements satisfy the same algebraic properties as Dirac matrices [22]. The basis vectors  $\gamma_\mu$  determine a unique pseudoscalar  $I = \gamma_0\gamma_1\gamma_2\gamma_3 = \mathbf{e}_1\mathbf{e}_2\mathbf{e}_3$ , with the properties  $I^2 = -1$  and  $\gamma_\mu I = -I\gamma_\mu$ . The two spins  $Is_1(\lambda)$  and  $Is_2(\lambda)$  are now spacetime covariant objects. They originate in the overlap of the backward light cones of Alice and Bob, along with the initial state  $\lambda$ , as shown in Fig. 1.

We now wish to represent the measurements of these spins using the detectors  $Ia = Ia^\mu\gamma_\mu$  and  $Ib = Ib^\mu\gamma_\mu$ , which we also represent using 4-vectors in  $Cl_{1,3}$ , situated at a spacelike distance from each other, within the hypersurface  $S^3$ . Such a spacelike hypersurface can be specified in  $Cl_{1,3}$  using the timelike vector  $\gamma_0$ , representing our two observers:

$$Ia\gamma_0 = Ia^\mu\gamma_\mu\gamma_0 = Ia^0\gamma_0\gamma_0 + Ia^i\gamma_i\gamma_0 = a^0I + Ia^i\mathbf{e}_i = a^0I + I \cdot \mathbf{a} = a^0I + \mathbf{D}(\mathbf{a}) \quad (52)$$

$$\text{and } Ib\gamma_0 = Ib^\mu\gamma_\mu\gamma_0 = Ib^0\gamma_0\gamma_0 + Ib^i\gamma_i\gamma_0 = b^0I + Ib^i\mathbf{e}_i = b^0I + I \cdot \mathbf{b} = b^0I + \mathbf{D}(\mathbf{b}), \quad (53)$$

because  $\gamma_0^2 = 1$  and  $\gamma_i\gamma_0 = \mathbf{e}_i$  constitute the spatial basis vectors in the algebra  $Cl_{3,0}$  [22]. Such an observer-dependent projection of a 4-vector in  $Cl_{1,3}$  onto a (1+3)-dimensional space, resulting in a timelike scalar and a spacelike vector in  $Cl_{3,0}$ , is called a ‘‘spacetime split’’ in STA. Here  $I \cdot \mathbf{a} = \mathbf{D}(\mathbf{a})$  and  $I \cdot \mathbf{b} = \mathbf{D}(\mathbf{b})$  are spacelike bivectors in  $Cl_{3,0}$ , analogous to those in Eqs. (50) and (51). We will use  $\mathbf{D}(\mathbf{a})$  and  $\mathbf{D}(\mathbf{b})$  to represent the two detectors of Alice and Bob.

Now, since the spins are measured by the above detectors, we must project them as well onto the hypersurface  $S^3$ :

$$Is_1(\lambda)\gamma_0 = Is_1^\mu(\lambda)\gamma_\mu\gamma_0 = Is_1^0\gamma_0\gamma_0 + \lambda Is_1^i\gamma_i\gamma_0 = s_1^0I + \lambda Is_1^i\mathbf{e}_i = s_1^0I + \lambda I \cdot \mathbf{s}_1 = s_1^0I + \mathbf{L}(\mathbf{s}_1, \lambda) \quad (54)$$

$$\text{and } Is_2(\lambda)\gamma_0 = Is_2^\mu(\lambda)\gamma_\mu\gamma_0 = Is_2^0\gamma_0\gamma_0 + \lambda Is_2^i\gamma_i\gamma_0 = s_2^0I + \lambda Is_2^i\mathbf{e}_i = s_2^0I + \lambda I \cdot \mathbf{s}_2 = s_2^0I + \mathbf{L}(\mathbf{s}_2, \lambda). \quad (55)$$

Next, we set up the time coordinate from  $-t$  to 0 in Figs. 1 and 2, where  $-t$  is the instant at which the singlet state is produced from the source in the overlap of the backward light cones of Alice and Bob, and 0 is the instant at which the constituent spins  $s_1^0I + \mathbf{L}(\mathbf{s}_1, \lambda)$  and  $s_2^0I + \mathbf{L}(\mathbf{s}_2, \lambda)$  are measured *simultaneously* by the detectors  $a^0I + \mathbf{D}(\mathbf{a})$  and  $b^0I + \mathbf{D}(\mathbf{b})$ , respectively. Consequently, since  $a^0, b^0, s_1^0$ , and  $s_2^0$  can be identified as the respective time coordinates, in the coordinates in which the spins are measured simultaneously by Alice and Bob we must set  $a^0 = b^0 = s_1^0 = s_2^0 = 0$ , reducing the spin and detector 4-vectors within  $Cl_{1,3}$  to the bivectors  $\mathbf{L}(\mathbf{s}_1, \lambda)$ ,  $\mathbf{L}(\mathbf{s}_2, \lambda)$ ,  $\mathbf{D}(\mathbf{a})$ , and  $\mathbf{D}(\mathbf{b})$  within  $Cl_{3,0}$ . The two relativistic spins  $Is_1(\lambda)$  and  $Is_2(\lambda)$  that originate in the overlap of the backward light cones of Alice and Bob at time  $-t$  are thus detected as  $\mathbf{L}(\mathbf{s}_1, \lambda)$  and  $\mathbf{L}(\mathbf{s}_2, \lambda)$  at time 0 by the detectors  $\mathbf{D}(\mathbf{a})$  and  $\mathbf{D}(\mathbf{b})$ , respectively.

We are now in a position to derive the singlet correlation once again in a succinct and elegant manner. To this end, consider two measurement functions similar to (24) and (25), but now of the form

$$\pm 1 = \mathcal{A}(\mathbf{a}, \lambda^k): \mathbb{R}^3 \times \{\lambda^k\} \longrightarrow S^3 \hookrightarrow \mathbb{R}^4 \quad (56)$$

and

$$\pm 1 = \mathcal{B}(\mathbf{b}, \lambda^k): \mathbb{R}^3 \times \{\lambda^k\} \longrightarrow S^3 \hookrightarrow \mathbb{R}^4, \quad (57)$$

---

<sup>2</sup> In Geometric Algebra [10] bivectors are viewed as *directed* numbers and characterized by only three abstract properties: (1) a magnitude, (2) a direction (specified by a vector orthogonal to it), and (3) a sense of rotation. The bivector  $\mathbf{L}(\mathbf{a}, \lambda)$  thus specifies  $\pm 1$  spin about  $\mathbf{a}$ .

where  $\lambda^k = \pm 1$  for each run  $k$  of the experiment considered in Fig. 2. More explicitly, let the spin bivectors  $\mp \mathbf{L}(\mathbf{s}, \lambda^k)$  emerging from a common source be detected by two space-like separated detector bivectors  $\mathbf{D}(\mathbf{a})$  and  $\mathbf{D}(\mathbf{b})$ , giving

$$S^3 \ni \mathcal{A}(\mathbf{a}, \lambda^k) := \lim_{\mathbf{s}_1 \rightarrow \mathbf{a}} \{-\mathbf{D}(\mathbf{a}) \mathbf{L}(\mathbf{s}_1, \lambda^k)\} = \begin{cases} +1 & \text{if } \lambda^k = +1 \\ -1 & \text{if } \lambda^k = -1 \end{cases} \text{ with } \langle \mathcal{A}(\mathbf{a}, \lambda^k) \rangle = 0 \quad (58)$$

and

$$S^3 \ni \mathcal{B}(\mathbf{b}, \lambda^k) := \lim_{\mathbf{s}_2 \rightarrow \mathbf{b}} \{+\mathbf{L}(\mathbf{s}_2, \lambda^k) \mathbf{D}(\mathbf{b})\} = \begin{cases} -1 & \text{if } \lambda^k = +1 \\ +1 & \text{if } \lambda^k = -1 \end{cases} \text{ with } \langle \mathcal{B}(\mathbf{b}, \lambda^k) \rangle = 0, \quad (59)$$

where we assume the orientation  $\lambda$  of  $S^3$  to be a random variable with 50/50 chance of being  $+1$  or  $-1$  at the moment of the pair-creation, making the spinning bivector  $\mathbf{L}(\mathbf{n}, \lambda^k)$  a random variable *relative* to the detector bivector  $\mathbf{D}(\mathbf{n})$ :

$$\mathbf{L}(\mathbf{n}, \lambda^k) = \lambda^k \mathbf{D}(\mathbf{n}) \iff \mathbf{D}(\mathbf{n}) = \lambda^k \mathbf{L}(\mathbf{n}, \lambda^k). \quad (60)$$

It is important to recall here that an orientation of a manifold is a *relative* concept [12]. Within geometric algebra  $Cl_{3,0}$  the choice of the sign of the unit pseudoscalar amounts to choosing an orientation of the physical space [10, 11].

Despite being algebraically different expressions, the detection processes encoded by Eqs. (58) and (59) are effectively the same as those defined by Bell in his local model [2, 18] within  $\mathbb{R}^3$ , namely  $\mathcal{A}(\mathbf{a}, \lambda^k) \cong \text{sign}(+\mathbf{s}_1^k \cdot \mathbf{a}) = \pm 1$  and  $\mathcal{B}(\mathbf{b}, \lambda^k) \cong \text{sign}(-\mathbf{s}_2^k \cdot \mathbf{b}) = \pm 1$ . They pick out the normalized components of the two spins about the vectors  $\mathbf{a}$  and  $\mathbf{b}$ , representing two scalar points of the 3-sphere. To see this explicitly, we can expand the RHS of Eq. (58) as follows:

$$\lim_{\mathbf{s}_1 \rightarrow \mathbf{a}} \{-\mathbf{D}(\mathbf{a}) \mathbf{L}(\mathbf{s}_1, \lambda^k)\} = \lim_{\mathbf{s}_1 \rightarrow \mathbf{a}} \{-\lambda^k \mathbf{L}(\mathbf{a}, \lambda^k) \mathbf{L}(\mathbf{s}_1, \lambda^k)\} \quad (61)$$

$$= \lim_{\mathbf{s}_1 \rightarrow \mathbf{a}} [-\lambda^k \{-\mathbf{a} \cdot \mathbf{s}_1 - \mathbf{L}(\mathbf{a} \times \mathbf{s}_1, \lambda^k)\}] \quad (62)$$

$$= \lim_{\mathbf{s}_1 \rightarrow \mathbf{a}} \{+\mathbf{a} \cdot (\lambda^k \mathbf{s}_1) + I \cdot (\mathbf{a} \times \mathbf{s}_1)\} \quad (63)$$

$$\cong \text{sign}(+\mathbf{s}_1^k \cdot \mathbf{a}), \text{ with } \mathbf{s}_1^k \equiv \lambda^k \mathbf{s}_1, \quad (64)$$

where Eqs. (60), (49), and (50) are used. Likewise we can expand the RHS of Eq. (59) using Eqs. (60), (49), and (51):

$$\lim_{\mathbf{s}_2 \rightarrow \mathbf{b}} \{+\mathbf{L}(\mathbf{s}_2, \lambda^k) \mathbf{D}(\mathbf{b})\} = \lim_{\mathbf{s}_2 \rightarrow \mathbf{b}} \{+\mathbf{L}(\mathbf{s}_2, \lambda^k) \lambda^k \mathbf{L}(\mathbf{b}, \lambda^k)\} \quad (65)$$

$$= \lim_{\mathbf{s}_2 \rightarrow \mathbf{b}} [+ \lambda^k \{-\mathbf{s}_2 \cdot \mathbf{b} - \mathbf{L}(\mathbf{s}_2 \times \mathbf{b}, \lambda^k)\}] \quad (66)$$

$$= \lim_{\mathbf{s}_2 \rightarrow \mathbf{b}} \{-(\lambda^k \mathbf{s}_2) \cdot \mathbf{b} - I \cdot (\mathbf{s}_2 \times \mathbf{b})\} \quad (67)$$

$$\cong \text{sign}(-\mathbf{s}_2^k \cdot \mathbf{b}), \text{ with } \mathbf{s}_2^k \equiv \lambda^k \mathbf{s}_2. \quad (68)$$

Moreover, as demanded by the conservation of angular momentum, we require the total spin to respect the condition

$$-\mathbf{L}(\mathbf{s}_1, \lambda^k) + \mathbf{L}(\mathbf{s}_2, \lambda^k) = 0 \iff \mathbf{L}(\mathbf{s}_1, \lambda^k) = \mathbf{L}(\mathbf{s}_2, \lambda^k) \iff \mathbf{s}_1 = \mathbf{s}_2 \equiv \mathbf{s} \text{ [cf. Fig. 2]}. \quad (69)$$

Evidently, in the light of the product rule (49) for the unit bivectors, the above condition is equivalent to the condition

$$\mathbf{L}(\mathbf{s}_1, \lambda^k) \mathbf{L}(\mathbf{s}_2, \lambda^k) = \{\mathbf{L}(\mathbf{s}, \lambda^k)\}^2 = \mathbf{L}^2(\mathbf{s}, \lambda^k) = -1. \quad (70)$$

The expectation value of simultaneous outcomes  $\mathcal{A}(\mathbf{a}, \lambda^k) = \pm 1$  and  $\mathcal{B}(\mathbf{b}, \lambda^k) = \pm 1$  in  $S^3$  then works out as follows:

$$\mathcal{E}(\mathbf{a}, \mathbf{b}) = \lim_{n \rightarrow \infty} \left[ \frac{1}{n} \sum_{k=1}^n \mathcal{A}(\mathbf{a}, \lambda^k) \mathcal{B}(\mathbf{b}, \lambda^k) \right] \cong \lim_{n \rightarrow \infty} \left[ \frac{1}{n} \sum_{k=1}^n \text{sign}(+\mathbf{s}_1^k \cdot \mathbf{a}) \text{sign}(-\mathbf{s}_2^k \cdot \mathbf{b}) \right] \quad (71)$$

$$= \lim_{n \rightarrow \infty} \left[ \frac{1}{n} \sum_{k=1}^n \left[ \lim_{\mathbf{s}_1 \rightarrow \mathbf{a}} \{-\mathbf{D}(\mathbf{a}) \mathbf{L}(\mathbf{s}_1, \lambda^k)\} \right] \left[ \lim_{\mathbf{s}_2 \rightarrow \mathbf{b}} \{+\mathbf{L}(\mathbf{s}_2, \lambda^k) \mathbf{D}(\mathbf{b})\} \right] \right] \quad (72)$$

$$= \lim_{n \rightarrow \infty} \left[ \frac{1}{n} \sum_{k=1}^n \lim_{\substack{\mathbf{s}_1 \rightarrow \mathbf{a} \\ \mathbf{s}_2 \rightarrow \mathbf{b}}} \{-\mathbf{D}(\mathbf{a})\} \{\mathbf{L}(\mathbf{s}_1, \lambda^k) \mathbf{L}(\mathbf{s}_2, \lambda^k)\} \{+\mathbf{D}(\mathbf{b})\} \right] \quad (73)$$

$$= \lim_{n \rightarrow \infty} \left[ \frac{1}{n} \sum_{k=1}^n \lim_{\substack{s_1 \rightarrow \mathbf{a} \\ s_2 \rightarrow \mathbf{b}}} \{ -\lambda^k \mathbf{L}(\mathbf{a}, \lambda^k) \} \{ -1 \} \{ +\lambda^k \mathbf{L}(\mathbf{b}, \lambda^k) \} \right] \quad (74)$$

$$= \lim_{n \rightarrow \infty} \left[ \frac{1}{n} \sum_{k=1}^n \lim_{\substack{s_1 \rightarrow \mathbf{a} \\ s_2 \rightarrow \mathbf{b}}} \left\{ + (\lambda^k)^2 \mathbf{L}(\mathbf{a}, \lambda^k) \mathbf{L}(\mathbf{b}, \lambda^k) \right\} \right] \quad (75)$$

$$= \lim_{n \rightarrow \infty} \left[ \frac{1}{n} \sum_{k=1}^n \mathbf{L}(\mathbf{a}, \lambda^k) \mathbf{L}(\mathbf{b}, \lambda^k) \right] \quad (76)$$

$$= -\mathbf{a} \cdot \mathbf{b} - \lim_{n \rightarrow \infty} \left[ \frac{1}{n} \sum_{k=1}^n \mathbf{L}(\mathbf{a} \times \mathbf{b}, \lambda^k) \right] \quad (77)$$

$$= -\mathbf{a} \cdot \mathbf{b} - \lim_{n \rightarrow \infty} \left[ \frac{1}{n} \sum_{k=1}^n \lambda^k \right] \mathbf{D}(\mathbf{a} \times \mathbf{b}) \quad (78)$$

$$= -\mathbf{a} \cdot \mathbf{b} + 0. \quad (79)$$

Here Eq. (72) follows from Eq. (71) by substituting the functions  $\mathcal{A}(\mathbf{a}, \lambda^k)$  and  $\mathcal{B}(\mathbf{b}, \lambda^k)$  from the definitions (58) and (59); Eq. (73) follows from Eq. (72) by using the “product of limits equal to limits of product” rule [which can be verified by recognizing that the same quaternion  $-\mathbf{D}(\mathbf{a}) \mathbf{L}(\mathbf{a}, \lambda^k) \mathbf{L}(\mathbf{b}, \lambda^k) \mathbf{D}(\mathbf{b})$  results from the limits in Eqs. (72) and (73)]; Eq. (74) follows from Eq. (73) by (i) using the relation (60) [thus setting all bivectors in the spin bases], (ii) the associativity of the geometric product, and (iii) the conservation of spin angular momentum specified in Eq. (70); Eq. (75) follows from Eq. (74) by recalling that scalars such as  $\lambda^k$  commute with the bivectors; Eq. (76) follows from Eq. (75) by using  $\lambda^2 = +1$ , and by removing the superfluous limit operations; Eq. (77) follows from Eq. (76) by using the geometric product or identity (49), together with the fact that there is no third spin about the orthogonal direction  $\mathbf{a} \times \mathbf{b}$  once the two spins are already detected along the directions  $\mathbf{a}$  and  $\mathbf{b}$ ; Eq. (78) follows from Eq. (77) by using the relations (60) and summing over the counterfactual detections of the “third” spins about  $\mathbf{a} \times \mathbf{b}$ ; and Eq. (79) follows from Eq. (78) because the scalar coefficient of the bivector  $\mathbf{D}(\mathbf{a} \times \mathbf{b})$  vanishes in  $n \rightarrow \infty$  limit, since  $\lambda^k$  is a fair coin.

Note that, apart from the initial state  $\lambda^k$ , the only other assumption used in this derivation is that of the conservation of spin angular momentum (70). These two assumptions are necessary and sufficient to dictate the singlet correlations:

$$\mathcal{E}(\mathbf{a}, \mathbf{b}) = \lim_{n \rightarrow \infty} \left[ \frac{1}{n} \sum_{k=1}^n \mathcal{A}(\mathbf{a}, \lambda^k) \mathcal{B}(\mathbf{b}, \lambda^k) \right] = -\mathbf{a} \cdot \mathbf{b}. \quad (80)$$

This demonstrates that EPR-Bohm correlations are correlations among the scalar points of a quaternionic 3-sphere.

It is also instructive to evaluate the sum in Eq. (76) somewhat differently to bring out how the orientation  $\lambda^k$  plays an important role in the derivation of the above correlation. Instead of assuming  $\lambda^k = \pm 1$  to be an orientation of  $S^3$ , we may view it as specifying the ordering relation between the spin bivectors  $\mathbf{L}(\mathbf{a}, \lambda)$  and  $\mathbf{L}(\mathbf{b}, \lambda)$  and the detector bivectors  $\mathbf{D}(\mathbf{a})$  and  $\mathbf{D}(\mathbf{b})$  with 50/50 chance of occurring, and only subsequently identify it with an orientation of  $S^3$ :

$$\mathbf{L}(\mathbf{a}, \lambda = +1) \mathbf{L}(\mathbf{b}, \lambda = +1) = \mathbf{D}(\mathbf{a}) \mathbf{D}(\mathbf{b}) \quad (81)$$

or

$$\mathbf{L}(\mathbf{a}, \lambda = -1) \mathbf{L}(\mathbf{b}, \lambda = -1) = \mathbf{D}(\mathbf{b}) \mathbf{D}(\mathbf{a}). \quad (82)$$

Since the spins emerging from the source are oblivious to the detectors located at remote stations, we may represent spins with a trivector  $J$  and detectors with a trivector  $I$ , respectively, without assuming any relation between them:

$$\mathbf{L}(\mathbf{n}, \lambda) = J \cdot \mathbf{n} \quad (83)$$

and

$$\mathbf{D}(\mathbf{n}) = I \cdot \mathbf{n}, \quad (84)$$

for any given dual vector  $\mathbf{n}$ . We can now easily find the relationship between  $J$  and  $I$  using the identities (48) and

$$\mathbf{D}(\mathbf{a}) \mathbf{D}(\mathbf{b}) = -\mathbf{a} \cdot \mathbf{b} - \mathbf{D}(\mathbf{a} \times \mathbf{b}). \quad (85)$$

Substituting the right-hand sides of these identities into the ordering relations (81) and (82) reduces the relations to

$$-\mathbf{a} \cdot \mathbf{b} - \mathbf{L}(\mathbf{a} \times \mathbf{b}, \lambda = +1) = -\mathbf{a} \cdot \mathbf{b} - \mathbf{D}(\mathbf{a} \times \mathbf{b}) \quad (86)$$

or

$$-\mathbf{a} \cdot \mathbf{b} - \mathbf{L}(\mathbf{a} \times \mathbf{b}, \lambda = -1) = -\mathbf{b} \cdot \mathbf{a} - \mathbf{D}(\mathbf{b} \times \mathbf{a}) = -\mathbf{a} \cdot \mathbf{b} + \mathbf{D}(\mathbf{a} \times \mathbf{b}), \quad (87)$$

which, after canceling the scalar factor  $-\mathbf{a} \cdot \mathbf{b}$  and using  $\lambda = \pm 1$  and the definitions (83) and (84), further reduces to

$$\mathbf{L}(\mathbf{a} \times \mathbf{b}, \lambda) = \lambda \mathbf{D}(\mathbf{a} \times \mathbf{b}) \quad (88)$$

$$J \cdot (\mathbf{a} \times \mathbf{b}) = \lambda I \cdot (\mathbf{a} \times \mathbf{b}) \quad (89)$$

$$J = \lambda I. \quad (90)$$

We have thus proved that the ordering relations (81) and (82) between the spin bivectors  $\mathbf{L}(\mathbf{a}, \lambda)$  and  $\mathbf{L}(\mathbf{b}, \lambda)$  and the detector bivectors  $\mathbf{D}(\mathbf{a})$  and  $\mathbf{D}(\mathbf{b})$  are equivalent to our hypothesis that the orientation of the 3-sphere is a fair coin. Using the relations (49) and (88), together with the ordering relations (81) and (82), the sum (76) can now be evaluated directly by recognizing that the spins in the right and left oriented  $S^3$  satisfy the following geometrical relations [16, 17]:

$$\begin{aligned} \mathbf{L}(\mathbf{a}, \lambda^k = +1) \mathbf{L}(\mathbf{b}, \lambda^k = +1) &= -\mathbf{a} \cdot \mathbf{b} - \mathbf{D}(\mathbf{a} \times \mathbf{b}) \\ &= \mathbf{D}(\mathbf{a}) \mathbf{D}(\mathbf{b}) = (+I \cdot \mathbf{a})(+I \cdot \mathbf{b}) \end{aligned} \quad (91)$$

$$\begin{aligned} \text{and } \mathbf{L}(\mathbf{a}, \lambda^k = -1) \mathbf{L}(\mathbf{b}, \lambda^k = -1) &= -\mathbf{a} \cdot \mathbf{b} + \mathbf{D}(\mathbf{a} \times \mathbf{b}) = -\mathbf{b} \cdot \mathbf{a} - \mathbf{D}(\mathbf{b} \times \mathbf{a}) \\ &= \mathbf{D}(\mathbf{b}) \mathbf{D}(\mathbf{a}) = (+I \cdot \mathbf{b})(+I \cdot \mathbf{a}). \end{aligned} \quad (92)$$

In other words, when  $\lambda^k$  happens to be equal to  $+1$ ,  $\mathbf{L}(\mathbf{a}, \lambda^k) \mathbf{L}(\mathbf{b}, \lambda^k) = (+I \cdot \mathbf{a})(+I \cdot \mathbf{b})$ , and when  $\lambda^k$  happens to be equal to  $-1$ ,  $\mathbf{L}(\mathbf{a}, \lambda^k) \mathbf{L}(\mathbf{b}, \lambda^k) = (+I \cdot \mathbf{b})(+I \cdot \mathbf{a})$ . Consequently, the expectation value (71) reduces at once to

$$\mathcal{E}(\mathbf{a}, \mathbf{b}) = \frac{1}{2}(+I \cdot \mathbf{a})(+I \cdot \mathbf{b}) + \frac{1}{2}(+I \cdot \mathbf{b})(+I \cdot \mathbf{a}) = -\frac{1}{2}\{\mathbf{ab} + \mathbf{ba}\} = -\mathbf{a} \cdot \mathbf{b} + 0, \quad (93)$$

because the orientation  $\lambda^k$  of  $S^3$  is a fair coin. Here the last equality follows from the definition of the inner product. Given this result, it is not difficult to derive the corresponding upper bound on the expectation values within  $S^3$ , as we have demonstrated in section VIII:

$$|\mathcal{E}(\mathbf{a}, \mathbf{b}) + \mathcal{E}(\mathbf{a}, \mathbf{b}') + \mathcal{E}(\mathbf{a}', \mathbf{b}) - \mathcal{E}(\mathbf{a}', \mathbf{b}')| \leq 2\sqrt{2}. \quad (94)$$

We have verified both of these results in several numerical simulations [19, 20, 23–25]. The simulations are instructive on their own right and can be used for testing the effects of topology changes when the parameter  $\eta \in [0, \pi]$  is varied.

## VII. THE RAISON D'ÊTRE OF STRONG CORRELATIONS

Geometrically the above results can be understood in terms of the twist in the Hopf fibration of  $S^3 \cong \text{SU}(2)$ . Recall that locally (in the topological sense)  $S^3$  can be written as a product  $S^2 \times S^1$ , but globally it has no cross-section [26, 27]. It can be viewed also as a principal  $\text{U}(1)$  bundle over  $S^2$ , with the points of its base space  $S^2$  being the elements of the Lie algebra  $\text{su}(2)$ , which are pure quaternions, or bivectors [17, 28]. The product of two such bivectors are in general non-pure quaternions of the form (13), and are elements of the group  $\text{SU}(2)$  itself. That is to say, they are points of the bundle space  $S^3$ , whose elements are the preimages[26] of the points of the base space  $S^2$ . These preimages are 1-spheres,  $S^1$ , called Hopf circles, or Clifford parallels [29]. Since these 1-spheres are the fibers of the bundle, they do not share a single point in common. Each circle threads through every other circle in the bundle, making them linked together in a highly non-trivial configuration, which can be quantified by the following relation among the fibers [28]:

$$e^{i\psi_-} = e^{i\phi} e^{i\psi_+}, \quad (95)$$

where  $e^{i\psi_-}$  and  $e^{i\psi_+}$ , respectively, are the  $\text{U}(1)$  fiber coordinates above the two hemispheres  $H_-$  and  $H_+$  of the base space  $S^2$ , with spherical coordinates ( $0 \leq \theta < \pi$ ,  $0 \leq \phi < 2\pi$ );  $\phi$  is the angle parameterizing a thin strip  $H_- \cap H_+$

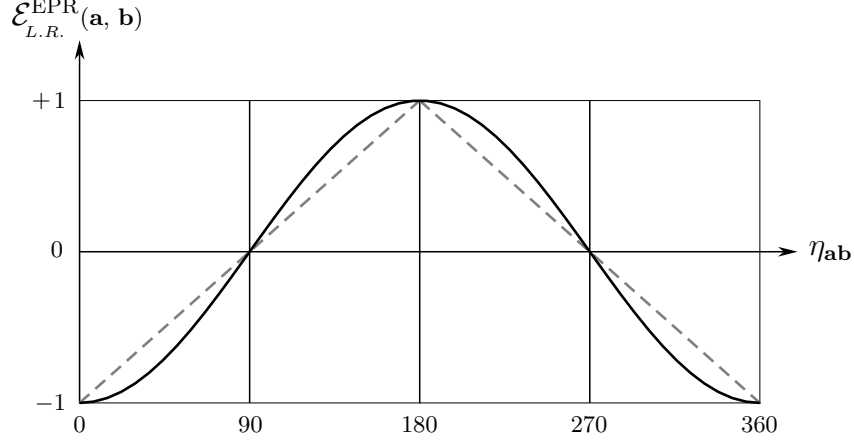


FIG. 3: Plot of an event-by-event numerical simulation of the EPR-Bohm correlations predicted by our  $S^3$  model [19, 20, 23–25].

around the equator of  $S^2$  [ $\theta \sim \frac{\pi}{2}$ ]; and  $e^{i\phi}$  is the transition function that glues the two sections  $H_-$  and  $H_+$  together, thus constituting the 3-sphere. It is evident from Eq. (95) that the fibers match perfectly at the angle  $\phi = 0$  (modulo  $2\pi$ ), but differ from each other at all intermediate angles  $\phi$ . For example,  $e^{i\psi_-}$  and  $e^{i\psi_+}$  differ by a minus sign at the angle  $\phi = \pi$ . Now in the Clifford-algebraic representation of our 3-sphere model the above relation can be written as

$$\{-\mathbf{D}(\mathbf{a})\mathbf{L}(\mathbf{s}_1, \lambda^k)\} = \{\mathbf{D}(\mathbf{a})\mathbf{D}(\mathbf{b})\} \{+\mathbf{L}(\mathbf{s}_2, \lambda^k)\mathbf{D}(\mathbf{b})\} \iff \mathbf{a}\mathbf{s} = \{\mathbf{a} \cdot \mathbf{b} + \mathbf{a} \wedge \mathbf{b}\} \mathbf{s}\mathbf{b}, \quad (96)$$

provided we identify the angles  $\eta_{\mathbf{a}\mathbf{s}_1}$  and  $\eta_{\mathbf{s}_2\mathbf{b}}$  between  $\mathbf{a}$  and  $\mathbf{s}_1$  and  $\mathbf{s}_2$  and  $\mathbf{b}$  with the fibers  $\psi_-$  and  $\psi_+$ , and the angle  $\eta_{\mathbf{a}\mathbf{b}}$  between  $\mathbf{a}$  and  $\mathbf{b}$  with the generator of the transition function  $e^{i\phi}$  on the equator of  $S^2$ . The above representation of Eq. (95) is not as unusual as it may seem at first sight once we recall that geometric products of vectors and bivectors appearing in it are quaternions, and the quaternionic 3-sphere defined in Eq. (10) as a set of unit quaternions remains closed under multiplication. Indeed, as we saw in Eq. (13), each element of  $S^3$  can be parameterized to take the form

$$\mathbf{q}(\mathbf{u}, \mathbf{v}) = \cos(\eta_{\mathbf{u}\mathbf{v}}) + \frac{\mathbf{u} \wedge \mathbf{v}}{\|\mathbf{u} \wedge \mathbf{v}\|} \sin(\eta_{\mathbf{u}\mathbf{v}}) = \exp \left\{ \frac{\mathbf{u} \wedge \mathbf{v}}{\|\mathbf{u} \wedge \mathbf{v}\|} \eta_{\mathbf{u}\mathbf{v}} \right\}, \quad (97)$$

which in turn can always be decomposed into a product of two bivectors, say  $\beta(\mathbf{u})$  and  $\beta(\mathbf{v})$ , belonging to an  $S^2 \subset S^3$ :

$$-\beta(\mathbf{u})\beta(\mathbf{v}) = -(\lambda I \cdot \mathbf{u})(\lambda I \cdot \mathbf{v}) = \mathbf{u}\mathbf{v} = \cos(\eta_{\mathbf{u}\mathbf{v}}) + \frac{\mathbf{u} \wedge \mathbf{v}}{\|\mathbf{u} \wedge \mathbf{v}\|} \sin(\eta_{\mathbf{u}\mathbf{v}}). \quad (98)$$

Multiplying both sides of (96) from the left with  $\mathbf{D}(\mathbf{a})$  and noting that all unit bivectors square to  $-1$ , we obtain

$$\mathbf{L}(\mathbf{s}_1, \lambda^k) = -\mathbf{D}(\mathbf{b})\mathbf{L}(\mathbf{s}_2, \lambda^k)\mathbf{D}(\mathbf{b}). \quad (99)$$

Next, multiplying the numerator and denominator on the RHS of this similarity relation with  $-\mathbf{D}(\mathbf{b})$  from the right and  $\mathbf{D}(\mathbf{b})$  from the left leads to the conservation of zero spin angular momentum, just as we have specified in Eq. (69):

$$\mathbf{L}(\mathbf{s}_1, \lambda^k) = \mathbf{L}(\mathbf{s}_2, \lambda^k) \iff \mathbf{L}(\mathbf{s}_1, \lambda^k)\mathbf{L}(\mathbf{s}_2, \lambda^k) = \mathbf{L}^2(\mathbf{s}, \lambda^k) = -1, \quad (100)$$

which was used in Eq. (74) to derive the strong correlations (80). We have thus shown that the conservation of spin angular momentum is not an additional assumption, but follows from the very geometry and topology of the 3-sphere.

Returning to the Hopf fibration of  $S^3$ , it is not difficult to see from Eq. (96) that if we set  $\mathbf{a} = \mathbf{b}$  (or equivalently  $\eta_{\mathbf{a}\mathbf{b}} = 0$ ) for all fibers, then  $S^3$  reduces to the trivial bundle  $S^2 \times S^1$ , since then the fiber coordinates  $\eta_{\mathbf{a}\mathbf{s}_1}$  and  $\eta_{\mathbf{s}_2\mathbf{b}}$  would match up exactly on the equator of  $S^2$  [ $\theta \sim \frac{\pi}{2}$ ]. In general, however, for  $\mathbf{a} \neq \mathbf{b}$ ,  $S^3 \neq S^2 \times S^1$ . For example, when  $\mathbf{a} = -\mathbf{b}$  (or equivalently when  $\eta_{\mathbf{a}\mathbf{b}} = \pi$ ) there will be a sign difference between the fibers at that point of the equator [26, 28]. That in turn would produce a twist in the bundle analogous to the twist in a Möbius strip. It is this

non-trivial twist in the  $S^3$  bundle that is responsible for the observed sign flips in the product  $\mathcal{A}\mathcal{B}$  of measurement events, from  $\mathcal{A}\mathcal{B} = -1$  for  $\mathbf{a} = \mathbf{b}$  to  $\mathcal{A}\mathcal{B} = +1$  for  $\mathbf{a} = -\mathbf{b}$ , as evident from the correlations (80), which are obtained in the limits  $\mathbf{s}_1 \rightarrow \mathbf{a}$  and  $\mathbf{s}_2 \rightarrow \mathbf{b}$ , together with  $\mathbf{s}_1 = \mathbf{s}_2 = \mathbf{s}$ , as in the definitions of the measurement functions (58) and (59). On the other hand, if the topology of our physical space were the trivial or product topology  $S^2 \times S^1$ , then the transition function  $\mathbf{ab}$  in Eq. (96) would be identical to  $+1$ , and we would not observe sign flips from  $\mathcal{A}\mathcal{B} = -1$  to  $\mathcal{A}\mathcal{B} = +1$  when  $\mathbf{a} = \mathbf{b}$  is rotated to  $\mathbf{a} = -\mathbf{b}$ . Moreover, in that case the limits  $\mathbf{s}_1 = \mathbf{s} \rightarrow \mathbf{a}$  and  $\mathbf{s}_2 = \mathbf{s} \rightarrow \mathbf{b}$  would also reinforce  $\mathbf{ab} = +1$  in Eq. (96), which in turn would lead only to  $\mathcal{A}\mathcal{B} = -1$  and never to  $\mathcal{A}\mathcal{B} = +1$ . Conversely, it is easy to see from the definitions (58) and (59) of  $\mathcal{A}$  and  $\mathcal{B}$  that, within the non-trivial topology of  $S^3$  necessitated by the general transition function  $\mathbf{ab}$  in (96), the relation  $\mathcal{A} = -\mathcal{B}$  by itself does not impose any restrictions, such as  $\mathbf{a} = \mathbf{b}$ , on the possible measurement directions  $\mathbf{a}$  and  $\mathbf{b}$  that Alice and Bob may wish to choose for their observations:

$$\mathcal{A}(\mathbf{a}, \lambda^k) = -\mathcal{B}(\mathbf{b}, \lambda^k) \quad (101)$$

$$\implies \lim_{\mathbf{s} \rightarrow \mathbf{a}} \{-\mathbf{D}(\mathbf{a}) \mathbf{L}(\mathbf{s}, \lambda^k)\} = -\lim_{\mathbf{s} \rightarrow \mathbf{b}} \{+\mathbf{L}(\mathbf{s}, \lambda^k) \mathbf{D}(\mathbf{b})\} \quad (102)$$

$$\implies \lim_{\mathbf{s} \rightarrow \mathbf{a}} \{-\lambda^k \mathbf{L}(\mathbf{a}, \lambda^k) \mathbf{L}(\mathbf{s}, \lambda^k)\} = -\lim_{\mathbf{s} \rightarrow \mathbf{b}} \{+\mathbf{L}(\mathbf{s}, \lambda^k) \lambda^k \mathbf{L}(\mathbf{b}, \lambda^k)\} \quad (103)$$

$$\implies \lim_{\mathbf{s} \rightarrow \mathbf{a}} [-\lambda^k \{-\mathbf{a} \cdot \mathbf{s} - \mathbf{L}(\mathbf{a} \times \mathbf{s}, \lambda^k)\}] = -\lim_{\mathbf{s} \rightarrow \mathbf{b}} [+\lambda^k \{-\mathbf{s} \cdot \mathbf{b} - \mathbf{L}(\mathbf{s} \times \mathbf{b}, \lambda^k)\}] \quad (104)$$

$$\implies \lim_{\mathbf{s} \rightarrow \mathbf{a}} \{+\lambda^k \mathbf{a} \cdot \mathbf{s} + I \cdot (\mathbf{a} \times \mathbf{s})\} = -\lim_{\mathbf{s} \rightarrow \mathbf{b}} \{-\lambda^k \mathbf{s} \cdot \mathbf{b} - I \cdot (\mathbf{s} \times \mathbf{b})\} \quad (105)$$

$$\implies \lambda^k \mathbf{a} \cdot \mathbf{a} = \lambda^k \mathbf{b} \cdot \mathbf{b} \quad (106)$$

$$\implies \|\mathbf{a}\|^2 = \|\mathbf{b}\|^2. \quad (107)$$

This result dictates that only the magnitudes but not the directions of the vectors  $\mathbf{a}$  and  $\mathbf{b}$  are constrained to be equal, despite the apparent anti-correlation between  $\mathcal{A}$  and  $\mathcal{B}$  in their very definitions (58) and (59). Alice and Bob are thus free to choose any angle between  $\mathbf{a}$  and  $\mathbf{b}$  on the unit 2-sphere, in harmony with the fibration (96) of  $S^3$ . The freedom to choose *any* directions  $\mathbf{a}$  and  $\mathbf{b}$  thus enables them to observe the twists in  $S^3$ , in the guise of strong correlations (80).

### VIII. DERIVATION OF TSIREL'SON'S BOUNDS ON THE STRENGTH OF CORRELATIONS

For completeness of our derivation of the correlation (79), in this section we derive the Tsirel'son's bounds in (94) on the strength of such correlations. To this end, consider four observation axes,  $\mathbf{a}$ ,  $\mathbf{a}'$ ,  $\mathbf{b}$ , and  $\mathbf{b}'$ , for the experiment illustrated in Fig. 2. Then the corresponding CHSH string of expectation values [16, 30], namely the correlator

$$\mathcal{E}(\mathbf{a}, \mathbf{b}) + \mathcal{E}(\mathbf{a}, \mathbf{b}') + \mathcal{E}(\mathbf{a}', \mathbf{b}) - \mathcal{E}(\mathbf{a}', \mathbf{b}'), \quad (108)$$

would be bounded by the constant  $2\sqrt{2}$ , as discovered by Tsirel'son within the setting of Clifford algebra applied to quantum mechanics within a Hilbert space. Here each of the joint expectation values of the measurement results  $\mathcal{A}(\mathbf{a}, \lambda) = \pm 1$  and  $\mathcal{B}(\mathbf{b}, \lambda) = \pm 1$  are defined as

$$\mathcal{E}(\mathbf{a}, \mathbf{b}) = \lim_{n \gg 1} \left[ \frac{1}{n} \sum_{k=1}^n \mathcal{A}(\mathbf{a}, \lambda^k) \mathcal{B}(\mathbf{b}, \lambda^k) \right], \quad (109)$$

with the measurement functions  $\mathcal{A}(\mathbf{a}, \lambda)$  and  $\mathcal{B}(\mathbf{b}, \lambda)$  defined in (58) and (59). But from (71) and (76) we also have the following geometrical and statistical identity:

$$\lim_{n \gg 1} \left[ \frac{1}{n} \sum_{k=1}^n \mathcal{A}(\mathbf{a}, \lambda^k) \mathcal{B}(\mathbf{b}, \lambda^k) \right] = \lim_{n \gg 1} \left[ \frac{1}{n} \sum_{k=1}^n \mathbf{L}(\mathbf{a}, \lambda^k) \mathbf{L}(\mathbf{b}, \lambda^k) \right]. \quad (110)$$

Using this identity the correlator (108) can now be rewritten as the following single average:

$$\lim_{n \gg 1} \left[ \frac{1}{n} \sum_{k=1}^n \{ \mathbf{L}(\mathbf{a}, \lambda^k) \mathbf{L}(\mathbf{b}, \lambda^k) + \mathbf{L}(\mathbf{a}, \lambda^k) \mathbf{L}(\mathbf{b}', \lambda^k) + \mathbf{L}(\mathbf{a}', \lambda^k) \mathbf{L}(\mathbf{b}, \lambda^k) + \mathbf{L}(\mathbf{a}', \lambda^k) \mathbf{L}(\mathbf{b}', \lambda^k) \} \right]. \quad (111)$$

But since the bivectors  $\mathbf{L}(\mathbf{a}, \lambda)$  and  $\mathbf{L}(\mathbf{b}, \lambda)$  are two independent equatorial points of  $S^3$ , we can take them to belong to two disconnected "sections" of  $S^3$  [*i.e.*, two disconnected  $\text{su}(2)$  2-spheres within  $S^3 \sim \text{SU}(2)$ ], satisfying

$$[\mathbf{L}(\mathbf{n}, \lambda), \mathbf{L}(\mathbf{n}', \lambda)] = 0 \quad \forall \mathbf{n} \text{ and } \mathbf{n}' \in \mathbb{R}^3, \quad (112)$$

which is equivalent to anticipating a null outcome along the direction  $\mathbf{n} \times \mathbf{n}'$  exclusive to both  $\mathbf{n}$  and  $\mathbf{n}'$ . If we now square the integrand of equation (111), use the above commutation relations, and use the fact that all unit bivectors square to  $-1$ , then the absolute value of the Bell-CHSH string (108) leads to the following variance inequality [16]:

$$|\mathcal{E}(\mathbf{a}, \mathbf{b}) + \mathcal{E}(\mathbf{a}, \mathbf{b}') + \mathcal{E}(\mathbf{a}', \mathbf{b}) - \mathcal{E}(\mathbf{a}', \mathbf{b}')| \leq \sqrt{\lim_{n \gg 1} \left[ \frac{1}{n} \sum_{k=1}^n \{4 + 4 \mathcal{T}_{\mathbf{a}\mathbf{a}'}(\lambda^k) \mathcal{T}_{\mathbf{b}'\mathbf{b}}(\lambda^k)\} \right]}, \quad (113)$$

where the classical commutators

$$\mathcal{T}_{\mathbf{a}\mathbf{a}'}(\lambda) := \frac{1}{2} [\mathbf{L}(\mathbf{a}, \lambda), \mathbf{L}(\mathbf{a}', \lambda)] = -\mathbf{L}(\mathbf{a} \times \mathbf{a}', \lambda) \quad (114)$$

and

$$\mathcal{T}_{\mathbf{b}'\mathbf{b}}(\lambda) := \frac{1}{2} [\mathbf{L}(\mathbf{b}', \lambda), \mathbf{L}(\mathbf{b}, \lambda)] = -\mathbf{L}(\mathbf{b}' \times \mathbf{b}, \lambda) \quad (115)$$

are the geometric measures of the torsion within  $S^3$ . Thus it is the non-vanishing torsion  $\mathcal{T}$  within the 3-sphere—*i.e.*, the parallelizing torsion which makes its Riemann curvature vanish—that is responsible for the stronger-than-linear correlation. We can see this from Eq. (113) by setting  $\mathcal{T} = 0$ , and in more detail as follows. By making a repeated use of the bivector identity

$$\mathbf{L}(\mathbf{a}, \lambda) \mathbf{L}(\mathbf{a}', \lambda) = -\mathbf{a} \cdot \mathbf{a}' - \mathbf{L}(\mathbf{a} \times \mathbf{a}', \lambda), \quad (116)$$

the above inequality can be further simplified to

$$\begin{aligned} |\mathcal{E}(\mathbf{a}, \mathbf{b}) + \mathcal{E}(\mathbf{a}, \mathbf{b}') + \mathcal{E}(\mathbf{a}', \mathbf{b}) - \mathcal{E}(\mathbf{a}', \mathbf{b}')| &\leq \sqrt{4 - 4(\mathbf{a} \times \mathbf{a}') \cdot (\mathbf{b}' \times \mathbf{b}) - 4 \lim_{n \gg 1} \left[ \frac{1}{n} \sum_{k=1}^n \mathbf{L}(\mathbf{z}, \lambda^k) \right]} \\ &\leq \sqrt{4 - 4(\mathbf{a} \times \mathbf{a}') \cdot (\mathbf{b}' \times \mathbf{b}) - 4 \lim_{n \gg 1} \left[ \frac{1}{n} \sum_{k=1}^n \lambda^k \right] \mathbf{D}(\mathbf{z})} \\ &\leq 2 \sqrt{1 - (\mathbf{a} \times \mathbf{a}') \cdot (\mathbf{b}' \times \mathbf{b}) - 0}, \end{aligned} \quad (117)$$

where  $\mathbf{z} = (\mathbf{a} \times \mathbf{a}') \times (\mathbf{b}' \times \mathbf{b})$ . The last two steps follow from the relation (60) between  $\mathbf{L}(\mathbf{z}, \lambda)$  and  $\mathbf{D}(\mathbf{z})$  and the fact that the orientation  $\lambda$  of  $S^3$  is evenly balanced between  $+1$  and  $-1$ . Finally, by noticing that trigonometry dictates

$$-1 \leq (\mathbf{a} \times \mathbf{a}') \cdot (\mathbf{b}' \times \mathbf{b}) \leq +1, \quad (118)$$

the above inequality can be reduced to the familiar form

$$|\mathcal{E}(\mathbf{a}, \mathbf{b}) + \mathcal{E}(\mathbf{a}, \mathbf{b}') + \mathcal{E}(\mathbf{a}', \mathbf{b}) - \mathcal{E}(\mathbf{a}', \mathbf{b}')| \leq 2\sqrt{2}. \quad (119)$$

Needless to say, this result can also be derived directly from the correlation (79):

$$|\mathcal{E}(\mathbf{a}, \mathbf{b}) + \mathcal{E}(\mathbf{a}, \mathbf{b}') + \mathcal{E}(\mathbf{a}', \mathbf{b}) - \mathcal{E}(\mathbf{a}', \mathbf{b}')| = |-\cos \eta_{\mathbf{a}\mathbf{b}} - \cos \eta_{\mathbf{a}\mathbf{b}'} - \cos \eta_{\mathbf{a}'\mathbf{b}} + \cos \eta_{\mathbf{a}'\mathbf{b}'}| \leq 2\sqrt{2}. \quad (120)$$

## IX. STANDARD INTERPRETATION OF BELL'S THEOREM IS RECOVERED IN $\mathbb{R}^3$ LIMIT

The  $S^3$  model presented above becomes conducive to the traditional interpretation of Bell's theorem when the algebraic, geometrical and topological properties of the compactified physical space  $S^3$  are ignored. In that case the upper bound of 2 on the Bell-CHSH inequality is respected. Thus, the results presented in this paper do not conflict with the standard interpretation of Bell's theorem outright but rather reproduces that interpretation as a special case in the flat geometry  $\mathbb{R}^3$  of the physical space, which is usually taken for granted in the literature on Bell's theorem. There are several different ways to appreciate this fact. As we saw in section V above, one way to appreciate it is by analyzing the even-by-event simulations presented therein [19, 20]. Another way to appreciating it is by noting that if we ignore the twist (70) or (100) in the Hopf bundle of  $S^3$ , then the value of the correlation function  $\mathcal{E}(\mathbf{a}, \mathbf{b})$  in (71) reduces to  $-1$  for all freely chosen parameters  $\mathbf{a}$  and  $\mathbf{b}$  for any initial state  $\lambda$ , and then the absolute bound of 2 on the Bell-CHSH correlator (94) is not exceeded. A third way to appreciate it is by setting the torsion  $\mathcal{T} = 0$  in Eq. (113) as noted between Eqs. (115) and (116) during the derivation of the Tsirel'son's bounds in section VIII. Each of these three ways provide different insights into how the standard interpretation of Bell's theorem is recovered in  $\mathbb{R}^3$  limit.

## X. THEORETICAL AND EXPERIMENTAL SUPPORT

In recent years there has been some theoretical and experimental support for the local-realistic model of the strong correlations presented above. For example, in an influential recent paper published in *Nature Communications* [31], the authors state that “Any no-go result, as for example Bell’s theorem, is phrased within a particular framework that comes with a set of built-in assumptions. Hence it is always possible that a theory evades the conclusions of the no-go result by not fulfilling these implicit assumptions.” This statement reflects a change in attitude of the physics community regarding the significance of Bell’s theorem for fundamental physics. In Bell’s local-realistic framework for the strong correlations [2], there are built-in assumptions about the algebraic, geometrical and topological properties of the physical space in which we are confined to perform all our experiments. In this paper we have relaxed some of these assumptions. It is therefore not surprising that we have been able to reproduce the singlet correlations exactly.

A more significant support for our locally causal model of the singlet correlations comes from a recently performed macroscopic experiment [32]. It provides an important experimental confirmation of the model presented above. The authors of the experiment write: “... we have demonstrated the violation of a Bell-type inequality using massive (around  $10^{10}$  atoms), macroscopic optomechanical devices, thereby verifying the nonclassicality of their state without the need for a quantum description of our experiment.” To be sure, by nonclassicality the authors mean violation of local realism, and support this orthodox interpretation by providing a quantum mechanical description of their massive, macroscopic, mechanical system. However, the key phrase also used by the authors to describe their experiment is the following: “... without the need for a quantum description of our experiment.” What this means is that we have an experimental proof that Bell-type inequalities can be violated also by purely classical, macroscopic systems without requiring a quantum mechanical description of the experiment. But that is exactly what our model presented above also predicts [16, 33]. According to our model, the violations of Bell inequalities are a result of the algebraic, geometrical, and topological properties of the compactified physical space,  $S^3$ . The concepts of quantum entanglement, non-locality, non-reality, or irreducible randomness are not necessary for explaining the violations of Bell inequalities.

## XI. CONCLUDING REMARKS

In this paper we have shown that it is possible to reproduce the statistical predictions of quantum mechanics in a locally causal manner, at least for the simplest entangled state such as the EPR-Bohm state. In particular, we have shown that such a locally causal description of the singlet state in the sense of Bell is possible at least within the spherical topology of a well known Friedmann-Robertson-Walker spacetime, viewed as a non-cosmological, terrestrial solution of Einstein’s field equations. More specifically, we have presented a local, deterministic, and realistic model within such a Friedmann-Robertson-Walker spacetime which describes simultaneous measurements of the spins of two fermions emerging in a singlet state from the decay of a spinless boson. We have then shown that the predictions of this locally causal model agree exactly with those of quantum theory, without needing data rejection, remote contextuality, superdeterminism, or backward causation. A Clifford-algebraic representation of the 3-sphere with vanishing spatial curvature and non-vanishing torsion then allows us to transform our model in an elegant form. Several event-by-event numerical simulations of the model have confirmed our analytical results with accuracy of at least 4 parts in  $10^4$  parts.

### Appendix: Formulation of Local Causality in the Manner of Bell

In this appendix we review the notion of local causality, as originally conceived by Einstein in the present context, and later formalized by Bell [2]. A more detailed discussion by Bell on the subject can be found in his last paper [21].

Our main goal here is to stress that the model constructed above is indeed locally causal in the sense of Einstein and Bell, despite the fact that it relies on the global topology of the spatial slices,  $S^3$ . It will also become evident from our discussion below that, although the correlation function  $\mathcal{E}(\mathbf{a}, \mathbf{b})$  is manifestly time-independent, the measurement functions  $\mathcal{A}(\mathbf{a}, \lambda)$  and  $\mathcal{B}(\mathbf{b}, \lambda)$  it depends on are themselves not time-independent. Indeed they depend on the initial states  $\lambda$  of the system specified at an earlier time and the final detector directions  $\mathbf{a}$  and  $\mathbf{b}$  chosen by Alice and Bob at a later time, as shown in Figs. 1 and 2. On the other hand, since we have set the scale factor  $a(t) = 1$  in the solution (9), the times elapsed between the initial and final instants of the experiments are obviously not cosmological epochs.



For deterministic models of the EPR-Bohm correlation (such as the one constructed above), Bell considered a joint observable of the form  $\mathcal{A}\mathcal{B}(\mathbf{a}, \mathbf{b}; \aleph, \lambda) = \pm 1$ , where  $\mathbf{a}$  and  $\mathbf{b}$ , respectively, are the freely chosen detector directions of Alice and Bob,  $\lambda$  is an initial or “complete” state of the singlet system (which is also referred to as a “common cause”, or “shared randomness”, or “hidden variable”), and  $\aleph$  stands for any number of other pre-established constants and/or variables pertaining to the experimental set up, which we shall refer to as *shared background*. Here two of the most important differences between the variables  $\{\mathbf{a}, \mathbf{b}\}$  and the variables  $\{\aleph, \lambda\}$  are: (1) while locally Alice and Bob have *total* control over the choice of variables  $\mathbf{a}$  and  $\mathbf{b}$  (respectively), they have *no* control over the variables  $\aleph$  and  $\lambda$  at any time during their experiment; and (2) while  $\aleph$  and  $\lambda$  are *completely specified* at an earlier time past the overlap of the backward lightcones of Alice and Bob (cf. Fig. 1), the variables  $\mathbf{a}$  and  $\mathbf{b}$  are freely chosen by them at a later time, as final directions along which the space-like separated measurement events  $\mathcal{A}(\mathbf{a}; \aleph, \lambda) = \pm 1$  and  $\mathcal{B}(\mathbf{b}; \aleph, \lambda) = \pm 1$  are determined. Bell called such events *locally explicable* if the joint observable  $\mathcal{A}\mathcal{B}(\mathbf{a}, \mathbf{b}; \aleph, \lambda) = \pm 1$  of Alice and Bob can be factorized into local parts as

$$\mathcal{A}\mathcal{B}(\mathbf{a}, \mathbf{b}; \aleph, \lambda) = \mathcal{A}(\mathbf{a}; \aleph, \lambda) \times \mathcal{B}(\mathbf{b}; \aleph, \lambda). \quad (\text{A.1})$$

Note that the functions  $\mathcal{A}(\mathbf{a}; \aleph, \lambda)$  and  $\mathcal{B}(\mathbf{b}; \aleph, \lambda)$  describe strictly local, realistic, and deterministically determined measurement events. Apart from the common cause  $\{\aleph, \lambda\}$ , which originates in the overlap of the backward lightcones of Alice and Bob as shown in Fig. 1, the event  $\mathcal{A} = \pm 1$  depends *only* on the measurement direction  $\mathbf{a}$  chosen freely by Alice; and analogously, apart from the common cause  $\{\aleph, \lambda\}$ , the event  $\mathcal{B} = \pm 1$  depends *only* on the measurement direction  $\mathbf{b}$  chosen freely by Bob. In particular, the function  $\mathcal{A}(\mathbf{a}; \aleph, \lambda)$  *does not* depend on either  $\mathbf{b}$  or  $\mathcal{B}$ , and the function  $\mathcal{B}(\mathbf{b}; \aleph, \lambda)$  *does not* depend on either  $\mathbf{a}$  or  $\mathcal{A}$ , just as demanded by Einstein’s notion of local causality [2, 21]. The correlation between the simultaneous measurement results  $\mathcal{A}(\mathbf{a}; \aleph, \lambda)$  and  $\mathcal{B}(\mathbf{b}; \aleph, \lambda)$  can then be computed as

$$\mathcal{E}(\mathbf{a}, \mathbf{b}) = \lim_{n \gg 1} \left[ \frac{1}{n} \sum_{k=1}^n \mathcal{A}(\mathbf{a}, \aleph, \lambda^k) \mathcal{B}(\mathbf{b}, \aleph, \lambda^k) \right]. \quad (\text{A.2})$$

Now in the case of the local model constructed above the shared background  $\aleph$  *includes* the topology  $\mathcal{T}$  of the spatial slices  $S^3$ . And this topology is *completely specified* from the outset, past the overlap of the backward lightcones of Alice and Bob. Therefore, Alice, for example, cannot influence either the freely chosen parameter  $\mathbf{b}$ , or the observed outcome  $\mathcal{B}$  of Bob by altering the topology, say, from  $\mathcal{T}$  to  $\mathcal{T}'$ . And likewise, Bob cannot influence either the freely chosen parameter  $\mathbf{a}$ , or the observed outcome  $\mathcal{A}$  of Alice by altering the topology from  $\mathcal{T}$  to  $\mathcal{T}'$  (e.g., from  $S^3$  to  $\mathbb{R}^3$ ). Thus, despite its reliance on the global topology of spatial slices, there is no violation of local causality in our model.

It is also evident from the prescription (A.2) that, quite appropriately, the shared background  $\aleph$  plays no role in the computation of the correlation. For this reason  $\aleph$  is usually dropped from the measurement functions by writing them simply as  $\mathcal{A}(\mathbf{a}, \lambda)$  and  $\mathcal{B}(\mathbf{b}, \lambda)$ , as we have done in this paper. On the other hand, from the above formulation of local causality it is evident that whether the joint outcome  $\mathcal{A}\mathcal{B}$  is  $+1$  or  $-1$  depends on the elapsed time between the initial instant when the state  $\lambda$  emerges from the source and the final instant when the measurements are made along the directions  $\mathbf{a}$  and  $\mathbf{b}$ , within a spacetime specified by the Friedmann-Robertson-Walker solution (9), with  $a(t) = 1$ .

### Acknowledgments

I am grateful to Fred Diether, Michel Fodje, Chantal Roth, and Albert Jan Wonnink for discussions and computing, and to Jay R. Yablon for the result (107), and for refuting some criticism of the derivation of (64). The first version of this paper (published on the arXiv) was written at Wolfson College of the University of Oxford.

- 
- [1] Einstein, A., Podolsky, B., Rosen, N.: Can quantum-mechanical description of physical reality be considered complete? *Phys. Rev.* **47**, 777-780 (1935).
  - [2] Bell, J. S.: On the Einstein-Podolsky-Rosen paradox. *Physics* **1**, 195-200 (1964).
  - [3] Clauser, J. F., Shimony, A.: Bell’s theorem: experimental tests, and implications. *Rep. Prog. Phys.* **41**, 1881-1927 (1978).
  - [4] Aspect, A., Grangier, P., Roger, G.: Experimental realization of Einstein-Podolsky-Rosen-Bohm gedankenexperiment: a new violation of Bell’s inequalities. *Phys. Rev. Lett.* **49**, 91-94 (1982).

- [5] Weihs, G., Jennewein, T., Simon, C., Weinfurter, H., Zeilinger, A.: Violation of Bell's inequality under strict Einstein locality conditions. *Phys. Rev. Lett.* **81**, 5039-5043 (1998).
- [6] Hensen, B. *et al.*: Loophole-free Bell inequality violation using electron spins separated by 1.3 kilometres. *Nature* **526**, 682-686 (2015).
- [7] Giustina, M. *et al.*: Significant loophole-free test of Bell's theorem with entangled photons. *Phys. Rev. Lett.* **115**, 250401 (2015).
- [8] Shalm, L. K. *et al.*: Strong loophole-free test of local realism. *Phys. Rev. Lett.* **115**, 250402 (2015).
- [9] Rauch, D. *et al.*: Cosmic Bell test using random measurement settings from high-redshift quasars. *Phys. Rev. Lett.* **121**, 080403 (2018).
- [10] Doran, C., Lasenby, A.: *Geometric Algebra for Physicists* (Cambridge University Press, Cambridge, 2003).
- [11] Dorst L, Fontijne D, Mann S.: *Geometric Algebra for Computer Science* (Elsevier, Amsterdam, 2007).
- [12] Christian, J.: Quantum correlations are weaved by the spinors of the Euclidean primitives. *R. Soc. Open Sci.* **5**, 180526; doi:10.1098/rsos.180526 (2018), arXiv:1806.02392; See also: Eight-dimensional Octonion-like but Associative Normed Division Algebra. <https://hal.archives-ouvertes.fr/hal-01933757v1> (2018).
- [13] Pearle, P. M.: Hidden-variable example based upon data rejection. *Phys. Rev. D* **2**, 1418-1425 (1970).
- [14] d'Inverno, R.: *Introducing Einstein's Relativity* (Clarendon Press, Oxford, 1992).
- [15] Nakahara, M.: *Geometry, Topology and Physics* (Adam Hilger, New York, 1990).
- [16] Christian, J.: Macroscopic observability of spinorial sign changes under  $2\pi$  rotations. *Int. J. Theor. Phys.* **54**, 20-46 (2015).
- [17] Christian, J.: *Disproof of Bell's Theorem: Illuminating the Illusion of Entanglement*, Second Edition (Browner Press, Boca Raton, Florida, 2014).
- [18] Peres, A.: *Quantum Theory: Concepts and Methods* (Kluwer, Dordrecht, 1993), p 161.
- [19] Christian, J.: A numerical simulation of the 3-sphere model for the EPR-Bohm correlation. Numerical computer simulation (2014). Available at <http://rpubs.com/jjc/13965> (Date of access: 08/02/2014).
- [20] Christian, J.: A three-dimensional simulation of the 3-sphere model for the EPR-Bohm correlation. Numerical computer simulation (2014). Available at <http://rpubs.com/jjc/16567> (Date of access: 04/04/2014).
- [21] Bell, J. S.: *La nouvelle cuisine*, in *Between Science and Technology* (ed. Sarlemijn, A., Kroes, P.) 97-115 (Elsevier Science Publishers, North-Holland, 1990).
- [22] Hestenes, D.: Spacetime physics with geometric algebra. *Am. J. Phys.* **71**, 691(2003).
- [23] Wonnink, A.-J.: GAVviewer code for the  $S^3$  model of the EPR-Bohm correlations (2015). Available at [http://challengingbell.blogspot.co.uk/2015/03/numerical-validation-of-vanishing-of\\_30.html](http://challengingbell.blogspot.co.uk/2015/03/numerical-validation-of-vanishing-of_30.html) (Date of access: 03/03/2015).
- [24] Diether III, C. F.: Improved GAVviewer code for the  $S^3$  model of the EPR-Bohm correlations (2015). Available at <http://challengingbell.blogspot.co.uk/2015/05/further-numerical-validation-of-joy.html> (Date of access: 03/04/2015).
- [25] Diether III, C. F.: Graph for the GAVviewer simulation of the  $S^3$  model for the EPR-Bohm correlations (2015). Available at <http://www.sciphysicsforums.com/spfbb1/viewtopic.php?f=6&t=200&p=5550#p5514> (Date of access: 03/04/2015).
- [26] Ryder, L. H.: Dirac monopoles and the Hopf map  $S^3$  to  $S^2$ . *J. Phys. A* **13**, 437-447 (1980).
- [27] Lyons, D. W.: An elementary introduction to the Hopf fibration. *Mathematical Magazine* **76**, 87-98 (2003).
- [28] Eguchi, T., Gilkey, P. B., Hanson, A. J.: *Gravitation, Gauge Theories and Differential Geometry*, Physics Reports, **66**, No. 6, 213 (1980) [cf. page 272, Eq. (4.21)].
- [29] Penrose, R.: *The Road to Reality: A Complete Guide to the Laws of the Universe* (Jonathan Cape, London, 2004).
- [30] Christian, J.: On a surprising oversight by John S. Bell in the proof of his famous theorem, arXiv:1704.02876 (2017).
- [31] Frauchiger, D. and Renner, R.: Quantum theory cannot consistently describe the use of itself, *Nature Communications*, **9**, 3711 (2018).
- [32] Marinković, I. *et al.*: Optomechanical Bell test, *Phys. Rev. Lett.*, **121**, 220404 (2018).
- [33] Christian, J.: Proposed macroscopic test of the physical relevance of Bell's theorem, [https://www.academia.edu/24765800/Proposed\\_Macroscopic\\_Test\\_of\\_the\\_Physical\\_Relevance\\_of\\_Bells\\_Theorem](https://www.academia.edu/24765800/Proposed_Macroscopic_Test_of_the_Physical_Relevance_of_Bells_Theorem) (2015).